Published in final edited form as:

Nat Immunol. 2017 February ; 18(2): 173–183. doi:10.1038/ni.3646.

Guidance of regulatory T cell development by Satb1-dependent super-enhancer establishment

Yohko Kitagawa[1,2], **Naganari Ohkura**[1], **Yujiro Kidani**[1], **Alexis Vandenbon**[3], **Keiji Hirota**[1,4], **Ryoji Kawakami**[1], **Keiko Yasuda**[1,2], **Daisuke Motooka**[5], **Shota Nakamura**[5], **Motonari Kondo**[6], **Ichiro Taniuchi**[7], **Terumi Kohwi-Shigematsu**[8], and **Shimon Sakaguchi**[1,2]

[1]Department of Experimental Immunology, WPI Immunology Frontier Research Center, Osaka University, Suita, Japan

[2]Laboratory of Experimental Immunology, Department of Regeneration Science and Engineering, Institute for Frontier Life and Medical Sciences, Kyoto University, Kyoto, Japan

[3]Immuno-Genomics Research Unit, WPI Immunology Frontier Research Center, Osaka University, Suita, Japan

[4]Laboratory of Integrative Biological Science, Department of Regeneration Science and Engineering, Institute for Frontier Life and Medical Sciences, Kyoto University, Kyoto, Japan

[5]Genome Information Research Center, Research Institute for Microbial Diseases, Osaka University, Suita, Japan

[6]Department of Molecular Immunology, School of Medicine, Toho University, Tokyo, Japan

[7]Laboratory for Transcriptional Regulation, Center for Integrative Medical Sciences, RIKEN, Yokohama, Japan

[8]Life Sciences Division, Lawrence Berkeley National Laboratory, Berkeley, California, USA

Abstract

Most Foxp3$^+$ regulatory T (T_{reg}) cells develop in the thymus as a functionally mature T cell subpopulation specialized for immune suppression. Their cell fate appears to be determined before *Foxp3* expression; yet molecular events that prime Foxp3$^-$ T_{reg} precursor cells are largely obscure. We found that T_{reg} cell–specific super-enhancers (T_{reg}-SEs), which were associated with *Foxp3* and other T_{reg} cell signature genes, began to be activated in T_{reg} precursor cells. T cell–specific

Correspondence should be addressed to S.S. (shimon@ifrec.osaka-u.ac.jp).

AUTHOR CONTRIBUTIONS

Y. Kitagawa designed, performed and analyzed most experiments, including flow cytometric analyses, *in vivo* and *in vitro* experiments, ChIP-seq, library preparation for sequencing and bioinformatics analyses. N.O. performed ATAC-seq and MBD-seq, Y. Kidani assisted with bioinformatical analyses and performed immunoblotting. A.V. and K.H. provided crucial advice. R.K. performed H3K4me3 ChIP-seq. K.Y. assisted with histological analysis. D.M. and S.N. performed amplicon sequencing. I.T. and T.K.-S. provided helpful suggestions. T.K.-S. and M.K. provided *Satb1* conditional knockout mouse. I.T. provided *Thpok*-Cre mouse. Y. Kitagawa and S.S. wrote the manuscript, and all authors reviewed it. T.K.-S. and N.O. critically read the manuscript and provided advice. S.S. supervised the project.

COMPETING FINANCIAL INTERESTS

The authors declare no competing financial interests.

Note: Any Supplementary Information and Source Data files are available in the online version of the paper.

deficiency of the genome organizer Satb1 impaired T_{reg}-SE activation and the subsequent expression of T_{reg} signature genes, causing severe autoimmunity due to T_{reg} cell deficiency. These results suggest that Satb1-dependent T_{reg}-SE activation is crucial for T_{reg} cell lineage specification in the thymus and that its perturbation is causative of autoimmune and other immunological diseases.

The majority of T_{reg} cells are produced in the thymus as a functionally distinct and mature T cell subpopulation that is actively involved in the maintenance of immunological self-tolerance and homeostasis[1]. They specifically express the transcription factor Foxp3, which has crucial roles in T_{reg} cell development and function[2–4]. In addition, T_{reg} cells acquire specific DNA hypomethylation patterns that are enriched at T_{reg} cell signature genes including *Foxp3*, *Il2ra*, *Ctla4* and *Ikzf2*. Acquisition of this epigenetic feature is independent of Foxp3 and associated with stable T_{reg}-specific gene expression required for T_{reg} cell lineage commitment and maintenance[5,6]. It is not clear, however, how T_{reg}-specific gene transcription and epigenetic changes are coordinately controlled in developing T_{reg} cells in the thymus.

Thymus-derived T_{reg} (tT_{reg}) cells develop mainly from immature $CD24^{hi}CD4^{+}CD8^{-}$ (CD4 single-positive (CD4SP)) thymocytes, with a minor fraction arising from $CD4^{+}CD8^{+}$ double-positive (DP) thymocytes[7]. Relatively strong agonistic T cell antigen receptor (TCR) stimulation and CD28 costimulation appear to generate $CD25^{+}GITR^{+}Foxp3^{-}$CD4SP tT_{reg} precursor cells[8]. TCR and IL-2 stimulation drive $CD25^{+}GITR^{+}Foxp3^{-}$CD4SP tT_{reg} precursor cells to differentiate into $Foxp3^{+}$ tT_{reg} cells that show the T_{reg} cell–type DNA hypomethylation pattern[8,9], but such stimulation does not generate T_{reg} cells from $CD25^{-}Foxp3^{-}$CD4SP thymocytes. These observations indicate that whether thymocytes will differentiate into T_{reg} cells is already determined at the tTreg precursor stage, before Foxp3 expression, posing the question of how tT_{reg} precursor cells are primed to differentiate into tT_{reg} cells at the transcriptional and epigenetic levels.

Cell differentiation is generally determined by the formation of the cell type–specific epigenetic landscape and the network of transcription factors[10,11]. Given that binding of most transcription factors depends on chromatin status, it is thought that the cell type–specific epigenetic landscape needs to be established before or concurrently with the expression of lineage-specifying transcription factors. In forming an epigenetic landscape, enhancer activation precedes promoter activation and associated gene expression[12]. Moreover, a number of studies have identified cell type–specific super-enhancers (SEs), which are defined as genomic regions with dense clustering of highly active enhancers, and demonstrated their association with the genes that define cell identity and determine cell lineage specification[13–16]. These findings suggest that the formation of a T_{reg} cell–specific enhancer landscape may be a key determinant of priming tT_{reg} precursor cells for tT_{reg} cell differentiation.

Here we address how T_{reg} cell lineage specification occurs before the expression of Foxp3 and other T_{reg} signature genes. We show that T_{reg}-SEs, which are associated with T_{reg} signature genes, are gradually established and activated in early stages of tT_{reg} cell development. Furthermore, we found that developmental stage–specific deletion of the

genome organizer Satb1 impairs T_{reg}-SE activation and fails to induce T_{reg} cell signature genes, thereby causing autoimmune diseases and IgE hyperproduction via tT_{reg} cell deficiency. Our results suggest that Satb1-dependent T_{reg}-SE activation is a crucial epigenetic event guiding tT_{reg} cell development.

RESULTS

Association of T_{reg}-SEs with T_{reg} signature genes

We first searched for SEs in the genomes of mouse $CD4^+CD25^+Foxp3^+$ T_{reg} and $CD4^+CD25^-Foxp3^-$ 'conventional' T (T_{conv}) cells by chromatin immunoprecipitation sequencing (ChIP-seq) of histone H3 acetylated at Lys27 (H3K27ac), an indicator of active enhancers. We used the algorithm ROSE[13,14] to stitch peaks within 12.5 kb and rank them by signal intensity. We plotted the H3K27ac signal against stitched enhancer rank and used the tangent of the resulting curve to distinguish between SEs and typical enhancers (TEs) (Fig. 1a) (details of SE definitions are given in Online Methods). Among 384 SEs thus defined in T_{reg} cells, 66 showed significantly (false discovery rate (FDR) < 0.05) higher H3K27ac signal intensity in T_{reg} cells (T_{reg}-SEs) and 318 were common to T_{reg} and T_{conv} cells (common-SEs); 37 among 355 SEs found in T_{conv} cells were specific to these cells (T_{conv}-SEs) (Fig. 1b). TEs were similarly grouped as T_{reg}-specific (T_{reg}-TEs), common (common-TEs) or T_{conv}-specific (T_{conv}-TEs).

When we compared the T_{reg}-SE region at the *Foxp3* locus in T_{reg} and T_{conv} cells, the former showed stronger H3K27ac and monomethylation of H3K4 (H3K4me1, an active enhancer mark when combined with H3K27ac)[17], greater chromatin accessibility (as determined by assay for transposase-accessible chromatin using sequencing (ATAC-seq)) and weaker H3K27me3 (an inactive enhancer mark) and DNA methylation (as indicated by methyl-CpG binding domain protein-enriched genome sequencing (MBD-seq)) (Fig. 1c). Average intensities of these signals at the 66 T_{reg}-SEs showed the same trends (Fig. 1d). Bidirectional enhancer RNAs, which are produced by active enhancers[18], showed significantly higher transcription at T_{reg}-SEs than at T_{reg}-TEs or the corresponding regions in T_{conv} cells (Fig. 1c,e). Multiple transcription factors, including Foxp3, Runx1, Bcl11b, Ets1 and CREB, which contribute to T_{reg} cell function in various ways[19], bound densely to T_{reg}-SEs (Fig. 1c and Supplementary Fig. 1a). Med1 and Smc1a, components of mediator and cohesin complexes, respectively, frequently co-occupied T_{reg}-SEs, indicating possible occurrences of promoter–enhancer looping within T_{reg}-SEs[20] (Fig. 1c and Supplementary Fig. 1a,b). T_{reg}-SEs were also enriched for T_{reg}-specific DNA demethylated regions, including hallmarks of T_{reg} cell identity at the *Foxp3*, *Ctla4* and *Ikzf2* loci[6] (Fig. 1f). Similarly to these findings with T_{reg}-SEs, H3K27ac density correlated with that of other 'permissive' epigenetic modifications at common-SEs, T_{conv}-SEs and TEs (Fig. 1e,f and Supplementary Fig. 1a–c).

Many T_{reg}-SEs were found in close proximity to T_{reg} signature genes, such as *Foxp3*, *Ctla4*, *Il2ra* and *Ikzf2* (Fig. 1a and Supplementary Data). Such T_{reg}-SE-associated genes showed higher expression in T_{reg} cells than in T_{conv} cells and higher expression than T_{reg}-TE-associated genes (Fig. 1g). Most of them also showed higher specificity for thymic and peripheral T_{reg} cells than for various immune cell types (Supplementary Fig. 1d). In addition, promoters of T_{reg}-SE-associated genes showed higher intensity of H3K4me3 (a

promoter activation mark) in T_{reg} cells than in T_{conv} cells (Fig. 1c,d). In contrast, common-SEs were associated with genes expressed similarly in T_{reg} and T_{conv} cells; further, the genes associated with T_{conv}-SEs included those downregulated in T_{reg} cells (Supplementary Fig. 1e).

Notably, the corresponding T_{reg}-SE regions in T_{conv} cells possessed H3K4me1 and H3K27me3 marks, with chromatin accessibility and binding of transcription factors, indicating their poised states[17] (Fig. 1c,d). However, TCR and IL-2 stimulation did not activate T_{reg}-SEs in T_{conv} cells or alter them in T_{reg} cells (Fig. 1h). These results, taken together, demonstrate highly specific and robust establishment of T_{reg}-SEs in T_{reg} cells and a strong correlation between T_{reg}-SE activity and associated gene expression, which suggests important roles of T_{reg}-SEs in T_{reg}-specific gene transcription.

T_{reg}-SE activation before *Foxp3* expression

We next examined the timing of T_{reg}-SE establishment in the course of *in vivo* tT_{reg} cell development. In DP and immature CD4SP thymocytes, T_{reg}-SE regions were marked with permissive H3K4me1 and repressive H3K27me3 modifications, which together indicated their poised state[17], as shown at the merged T_{reg}-SEs (Fig. 2a) and at the representative *Foxp3* gene locus (Fig. 2b). In tT_{reg} precursor cells, T_{reg}-SEs showed increased H3K27ac, decreased H3K27me3 and no changes in H3K4me1, indicating that they had begun to be activated (Fig. 2a–d and Supplementary Figs. 2a and 3a). These changes were intensified at the thymic T_{reg} cell stage. More detailed analyses revealed that approximately half of the T_{reg}-SEs showed significant (FDR < 0.05) increases in H3K27ac signal in tT_{reg} precursor cells before *Foxp3* expression, whereas others were activated at the thymic T_{reg} cell stage (Fig. 2d,e). The former included T_{reg}-SEs at *Foxp3* and other T_{reg} cell signature gene loci (Fig. 2b,f). These changes at T_{reg}-SE regions preceded chromatin loosening, DNA demethylation, activation of associated promoters and transcription of associated genes (Fig. 2a–c and Supplementary Figs. 2a and 3a). Furthermore, from early stages of tT_{reg} cell development, enhancer activity was stronger at T_{reg}-SEs than at T_{reg}-TEs, which probably facilitates robust induction of T_{reg}-SE-associated genes (Supplementary Fig. 2b). In contrast with T_{reg}-SEs, common-SEs were active in all tT_{reg} differentiation stages, whereas most T_{conv}-SEs were activated only in peripheral T_{conv} cells and maintained at a poised state in developing tT_{reg} cells, as shown for merged SEs (Supplementary Fig. 2c) and for each representative SE (Supplementary Fig. 3b,c). Thus, a series of chromatin configuration changes occurred specifically at T_{reg}-SEs in the course of tT_{reg} cell development, before the expression of *Foxp3*.

Potential of Satb1 as a pioneer factor

Next, to investigate the roles of T_{reg}-SEs during tT_{reg} cell differentiation *in vivo*, we searched for potential regulators of T_{reg}-SEs by expression analysis of epigenetic modifiers (GO terms chromatin organization (QuickGO GO:0006325) and epigenetic regulation of gene expression (QuickGO GO:0040029)). On the basis of the assumption that pioneer factors able to open up condensed chromatin would be required for an initial phase of cell differentiation[21,22], we selected epigenetic modifiers that showed significantly higher mRNA expression in tT_{reg} precursor cells than in peripheral T_{reg} cells (Fig. 3a). The most

differentially expressed epigenetic modifier was *Satb1*, which encodes a genome organizer that regulates both transcriptional and epigenetic changes in T cells by forming long-range chromatin loops, bringing distal genes together and recruiting epigenetic modifying enzymes and transcriptional machineries to target gene loci[23,24]. *Satb1* was also one of the few candidate genes that were upregulated toward the CD4SP stage, where most T_{reg} cells developed (Fig. 3b). It was expressed from the DP stage, further upregulated in immature CD4SP thymocytes and downregulated as T_{reg} cells differentiated (Fig. 3c). This pattern of *Satb1* expression, which precedes *Foxp3* expression, suggests a potential role of Satb1 in priming T_{reg}-SEs for T_{reg} cell differentiation.

We then examined the potential of Satb1 (or a Satb1-containing complex) as a pioneer factor for establishing T_{reg}-SEs. Satb1 ChIP-seq revealed that Satb1 bound to most T_{reg}-SEs, common-SEs and T_{conv}-SEs in DP, CD4SP and developing tT_{reg} cells (tT_{reg} precursor and thymic T_{reg} cells combined) but not in mature T_{reg} cells (Fig. 4a and Supplementary Fig. 4a). Moreover, 27% of Satb1-binding sites within T_{reg}-SEs at the DP stage were present in closed chromatin regions where ATAC-seq signal was low, indicating that Satb1, unlike typical transcription factors, can bind to closed chromatin. The Satb1-binding sites in open chromatin regions at the DP stage accompanied H3K27ac modification at flanking nucleosomes (Fig. 4b–d). In contrast, those in closed chromatin regions, notably present in T_{reg}-SEs at most T_{reg} cell signature gene loci, were not yet H3K27ac-modified and scarcely bound by transcription factors at the DP stage, showing gradual chromatin opening and H3K27ac modification from the tT_{reg} cell precursor stage. The former Satb1-bindng sites, which were enriched for Ets family binding motifs, were indeed bound by Ets1 and other transcription factors from the DP stage, whereas the latter was not enriched for any of ~2,000 motifs examined (Supplementary Fig. 4b). At the *Foxp3* locus, for example, Satb1 binding to closed chromatin first occurred at a newly identified conserved noncoding sequence (CNS), denoted as CNS0, in DP thymocytes. Satb1 subsequently bound to CNS3, an enhancer required for efficient *Foxp3* transcription[25], in CD4SP thymocytes, and to the TSS and CNS2, an enhancer specifically demethylated in T_{reg} cells and stabilizing *Foxp3* expression[5], in tT_{reg} precursor and thymic T_{reg} cells. This sequential binding of Satb1 along tT_{reg} cell development suggested that Satb1 might be involved in chromatin looping among regulatory regions initiated at CNS0.

These results demonstrate that Satb1 binds to T_{reg}-SEs and other SEs from the DP stage and suggest that a Satb1-containing complex could serve as a pioneer factor that initiates chromatin configuration changes of key T_{reg}-SE regions and regulates subsequent transcriptional and epigenetic changes of T_{reg} signature genes.

Defective tT_{reg} cell development by *Satb1* deletion

To further elucidate the role of Satb1 in T_{reg}-SE establishment and tT_{reg} cell development, we ablated Satb1 protein expression from the DP stage onwards by crossing mice bearing a *loxP*-flanked *Satb1* (*Satb1*$^{fl/fl}$) with mice expressing Cre recombinase from the *Cd4* promoter (*Cd4*-Cre^{+})[26] (Fig. 5a). Notably, CD25^{+}Foxp3^{+} T_{reg} cells were almost completely absent in both the thymus and the spleen of neonatal *Satb1*$^{fl/fl}$*Cd4*-Cre^{+} mice (Fig. 5b). *Satb1* deletion reduced the efficiency of thymocyte differentiation into CD4SP thymocytes

by approximately 50% (data not shown), but it particularly affected tT_{reg} cell development, as indicated by a significant reduction in the number and percentage of $Foxp3^+$ cells among CD4SP thymocytes (Fig. 5c). The deficiencies of $CD25^+Foxp3^+$CD4SP thymocytes and splenic $CD25^+Foxp3^+CD4^+$ T cells persisted for 14 d and 7 d, respectively, then recovered (Fig. 5d). Despite the age-dependent recovery of T_{reg} cell percentages, $CD25^+Foxp3^+$ T cells in the thymus of adult *Satb1*$^{fl/fl}$*Cd4*-Cre$^+$ mice were confined to the $CD24^-$ mature fraction (i.e., lacking $CD24^+$ immature T_{reg} cells found in wild-type thymus) and highly activated (Fig. 5e and Supplementary Fig. 5a,b). Mixed bone marrow chimeras prepared by reconstituting irradiated *Rag2*$^{-/-}$ mice with T cell–depleted bone marrow cells from CD45.1$^+$ wild-type mice and CD45.2$^+$ *Satb1*$^{fl/fl}$*Cd4*-Cre$^+$ mice also showed that *Satb1* deletion severely reduced thymic production of $Foxp3^+$ T cells (Fig. 5f). The production remained impaired 12 weeks after bone marrow reconstitution, indicating that both early and late waves of thymic T_{reg} cell development[27] were defective in *Satb1*$^{fl/fl}$*Cd4*-Cre$^+$ mice (data not shown). In addition, amplicon sequencing of bisulfite-treated DNA from wild-type or Satb1-deficient thymocytes in the chimeras revealed that *Satb1* deletion not only impaired Foxp3 induction but also T_{reg} cell–specific DNA demethylation (Fig. 5g).

The presence of mature peripheral $Foxp3^+$ cells despite impaired thymic T_{reg} cell production prompted us to examine their functional and phenotypic properties. Peripheral $Foxp3^+$ cells in *Satb1*$^{fl/fl}$*Cd4*-Cre$^+$ mice consisted of $CD25^+$ and $CD25^-$ populations (Fig. 5b). Satb1-deficient $CD25^+Foxp3^+$ cells, when compared with wild-type T_{reg} cells, showed similar *in vitro* suppressive activity, expression of T_{reg} cell signature genes, T_{reg} cell–specific DNA hypomethylation patterns and stability of *Foxp3* expression after *in vitro* TCR stimulation (Supplementary Fig. 5b–e). In contrast, Satb1-deficient $CD25^-Foxp3^+$ cells did not show these properties, which suggests that they might be T_{conv} cells with de-repressed Foxp3 expression. In addition, $CD25^+Foxp3^+$ cells from *Satb1*$^{fl/fl}$*Cd4*-Cre$^+$ mice contained $Nrp1^-Helios^-$ cells at an increased frequency (Supplementary Fig. 5f). As the low expression of Nrp1 and Helios marks peripherally induced T_{reg} (pT_{reg}) cells under a noninflammatory condition[28–30], we examined the mixed bone marrow chimeras and found that Satb1-deficient $CD25^+Foxp3^+$ cells were mostly $Nrp1^-Helios^-$ (Fig. 5h). These results suggest that, although *Satb1* deletion severely impaired tT_{reg} cell development, it allowed and even enhanced the development of pT_{reg} cells, and that some of them had recirculated to the thymus as $CD24^-Foxp3^+$ T cells[31] (Fig. 5e).

To further elucidate the differential effects of Satb1 on tT_{reg} and pT_{reg} cell development and the possible role of Satb1 for *Foxp3* repression in T_{conv} cells, we ablated Satb1 specifically in mature $CD4^+$ T cells after tT_{reg} cell development but before pT_{reg} cell differentiation by preparing *Satb1*$^{fl/fl}$*Thpok*-Cre$^+$ mice[32] (Supplementary Fig. 6a). This *Satb1* deletion did not affect tT_{reg} cell development (Fig. 5i) but de-repressed *Foxp3* expression in T_{conv} cells without evoking expression of other T_{reg} cell signature molecules or inducing T_{reg} cell–specific DNA demethylation (Supplementary Fig. 6b–d). Notably, despite no Satb1 binding at the *Foxp3* locus in wild-type T_{conv} cells, H3K27ac in the T_{reg}-SE of *Foxp3* was enhanced in both $CD25^-Foxp3^-$ and $CD25^-Foxp3^+$ cells from *Satb1*$^{fl/fl}$*Thpok*-Cre$^+$ mice, which suggests that Satb1 deficiency indirectly activated T_{reg}-SE to de-repress *Foxp3* expression (Supplementary Fig. 6e). *Satb1*$^{fl/fl}$*Thpok*-Cre$^+$ mice also showed an increased proportion of $Nrp1^-Helios^-CD25^+Foxp3^+$ pT_{reg} cells, which possessed T_{reg} cell–specific DNA

hypomethylation at the *Foxp3* CNS2 region to a similar extent as in wild-type pT_{reg} cells (Supplementary Fig. 6d,f). Moreover, when colitis was induced in *Rag2*$^{-/-}$ mice by cell transfer of wild-type and Satb1-deficient naive T cells, a significantly higher percentage ($P < 0.0001$) of T_{reg} cells with both Foxp3 expression and T_{reg} cell–specific DNA hypomethylation was generated from the Satb1-deficient fraction (Supplementary Fig. 6g,h). These results confirm that *Satb1* deletion de-represses *Foxp3* expression in mature T_{conv} cells and facilitates pT_{reg} cell differentiation.

Next, to address whether Satb1 is also required for T_{reg} cell maintenance, we deleted *Satb1* in differentiated T_{reg} cells from the Foxp3$^+$ thymic T_{reg} cell stage onwards by generating *Satb1*$^{fl/fl}$*Foxp3*-Cre$^+$ mice. Those mice did not show any significant changes in T_{reg} cell ratio or phenotype, which indicates that Satb1 is not required for the maintenance of T_{reg} cells (Fig. 5j and Supplementary Fig. 6i–k).

Notably, *Satb1*$^{fl/fl}$*Cd4*-Cre$^+$ but not *Satb1*$^{fl/fl}$*Thpok*-Cre$^+$ or *Satb1*$^{fl/fl}$ *Foxp3*-Cre$^+$ mice spontaneously developed histologically and serologically evident autoimmune or inflammatory disease in various organs including the ovaries, Langerhans islets, the salivary glands, the lung and the stomach (Fig. 6a,b). The tissue lesions could be adoptively transferred by splenocytes into syngenic *Rag2*$^{-/-}$ mice (Fig. 6c). They also showed significant elevation of serum IgE and increase of interferon-γ (IFN-γ)-producing CD4$^+$ T cells (Fig. 6d,e). We observed severe reductions in total T_{reg} cells, especially during the neonatal period as shown above, whereas wild-type and *Satb1*$^{fl/fl}$*Cd4*-Cre$^+$ mice showed no substantial difference in the efficiency of negative selection of self-reactive T_{conv} cells (Supplementary Fig. 5g). Moreover, transfer of wild-type Foxp3$^+$ T_{reg} cells into 4-d-old *Satb1*$^{fl/fl}$*Cd4*-Cre$^+$ mice at a marginal dose (1×10^6 cells) significantly prevented histological development of autoimmune disease and IgE hyper-production (Fig. 6a,b,d,e).

Taken together, these results indicate that the timing of *Satb1* deletion determines its effect on T_{reg} cell development. Its ablation in thymocytes before *Foxp3* expression predominantly impairs tT_{reg} cell development, whereas its deficiency in mature T_{conv} cells seems to promote pT_{reg} cell differentiation. In addition, impairment of tT_{reg} cell differentiation via *Satb1* deletion results in the development of autoimmune and other immunological diseases, despite enhanced generation of pT_{reg} cells.

T_{reg}-SE activation for T_{reg} cell development

Next, to determine how *Satb1* deletion would impair tT_{reg} cell development, we assessed the potential of Satb1-deficient tT_{reg} precursor cells to differentiate into thymic T_{reg} cells. Despite tT_{reg} cell deficiency, the tT_{reg} precursor cell fraction was higher in percentage in *Satb1*$^{fl/fl}$*Cd4*-Cre$^+$ mice than in *Satb1*$^{fl/+}$*Cd4*-Cre$^+$ littermates and had a similar cell surface phenotype (Fig. 7a,b and Supplementary Fig. 7a). Upon *in vitro* stimulation with IL-2 for 24 h (ref. 8), ~30% of tT_{reg} precursor cells from *Satb1*$^{fl/+}$*Cd4*-Cre$^+$ mice were Foxp3$^+$; however, a significantly lower percentage of the Satb1-deficient counterparts became Foxp3$^+$ (Fig. 7c,d). After IL-2 and TCR stimulation for 5 d (refs. 8,9), tT_{reg} precursor cells from *Satb1*$^{fl/+}$*Cd4*-Cre$^+$ mice differentiated into Foxp3$^+$ T cells with T_{reg} cell–specific DNA hypomethylation, whereas those from *Satb1*$^{fl/fl}$*Cd4*-Cre$^+$ mice did not (Fig. 7e,f). In addition, CD25$^-$Foxp3$^+$CD4SP thymocytes, another T_{reg} precursor population[33], were

substantially reduced in *Satb1*$^{fl/fl}$*Cd4*-Cre^{+} mice (Fig. 7a and Supplementary Fig. 7b). Moreover, Satb1-deficient CD25^{-}Foxp3^{+}CD4SP cells showed unstable Foxp3 expression after *in vitro* TCR stimulation, unlike their wild-type counterparts (Supplementary Fig. 7c).

To determine then whether the loss of T_{reg} cell differentiation potential in Satb1-deficient tT_{reg} precursor cells could be attributed to impaired T_{reg}-SE activation, we assessed the activation status of T_{reg}-SEs, which are normally active at the tT_{reg} precursor cell stage. Wild-type and Satb1-deficient DP cells and immature CD4SP cells showed similar intensities of H3K4me1, whereas Satb1-deficient tT_{reg} precursor cells showed much lower H3K27ac intensity than their wild-type counterparts (Fig. 8a,b and Supplementary Fig. 7d). The reduction occurred 'preferentially' at T_{reg}-SE regions to which Satb1 bound before chromatin opening (Fig. 8c and Supplementary Fig. 7e,f). For example, activation of T_{reg}-SE at the *Foxp3* locus did not increase beyond the level observed at the DP stage in Satb1-deficient thymocytes, most notably around CNS0, where Satb1 initially bound when chromatin was closed. In contrast, the effects of *Satb1* deletion on common-SEs and T_{conv}-SEs were less pronounced, making Satb1-deficient tT_{reg} precursor cells closer to immature CD4SP thymocytes in the principal component analysis of global H3K27ac pattern (Fig. 8d and Supplementary Fig. 7g,h). These results collectively indicate that stage-specific *Satb1* deletion 'preferentially' impairs activation of T_{reg}-SEs at the tT_{reg} precursor stage.

To examine the effects of this defective T_{reg}-SE activation on gene transcription, we compared the T_{reg}-SE activity in tT_{reg} precursor cells and CD24^{+}CD25^{+}CD4SP thymocyte gene expression (including tT_{reg} precursor and immature tT_{reg} cells) between wild-type and Satb1-deficient mice. Notably, among T_{reg}-SEs to which associated genes were assigned (59 out of 66 regions), there was a significant correlation between reduced T_{reg}-SE activity and impaired induction or upregulation of associated genes ($P < 0.00005$ in Fisher's exact test). Moreover, the genes associated with T_{reg}-SEs whose activity was downregulated by *Satb1* deletion showed significantly reduced expression when compared to the genes associated with other T_{reg}-SEs (Fig. 8e,f and Supplementary Fig. 8a,b). These genes included *Foxp3*, *Tnfrsf4* (encoding OX40), *Il2ra* (encoding CD25) and *Lrrc32* (encoding glycoprotein A repetitions predominant (GARP)).

Collectively, these data demonstrate a strong association between T_{reg}-SE establishment and subsequent T_{reg} cell–specific transcriptional changes during tT_{reg} cell development, which suggests a role for T_{reg}-SE activation in guiding T_{reg} cell lineage specification (Supplementary Fig. 8c).

DISCUSSION

The main findings of this report are that T_{reg}-SEs, associated with key T_{reg} cell signature genes, begin to be established in parallel before the expression of Foxp3 in the course of tT_{reg} cell development and that Satb1 deficiency before, but not after, the Foxp3^{+} thymic T_{reg} stage impairs T_{reg}-SE activation and, consequently, the expression of T_{reg} cell signature genes, causing severe autoimmunity.

SEs have been suggested to control the expression of the associated lineage-specifying genes in a number of cell types[13–16]. We found that T_{reg}-SEs were associated with the genes defining T_{reg} cell identity, such as *Foxp3*, *Ctla4* and *Il2ra*. In addition to the enriched transcription factor binding, we observed high transcription of enhancer RNAs from T_{reg}-SEs. Their contribution to increasing chromatin accessibility and promoting associated gene transcription[34] is one explanation for the enhanced transcription of associated genes. Moreover, frequent co-binding of Med1 and Smc1a, which indicates enhancer–promoter chromatin looping, suggests that multiple enhancers located within SEs regulate associated gene transcription via chromatin loop formation. These findings support the role of T_{reg}-SEs in inducing high expression of T_{reg} cell signature genes.

In the course of thymic T_{reg} cell development, T_{reg}-SE activation was initiated in parallel at most T_{reg} signature gene loci before their expression or T_{reg}-specific DNA demethylation[9]. This finding supports the contribution of T_{reg}-SEs in the induction of T_{reg} signature genes, and is in accord with findings that Foxp3 is not required for the induction of most T_{reg} signature genes but augments a pre-established pattern of gene expression in addition to its role as a repressor[6,35,36]. Moreover, T_{reg}-SEs were poised for activation in DP, immature CD4SP and peripheral T_{conv} cells, reflecting the potential of these cells to differentiate into T_{reg} cells with additional signals. These findings also suggest that certain molecules involved in T_{reg}-SE activation may be the true lineage specifying factors.

The pioneering effect of a Satb1-containing complex in T_{reg}-SE activation was corroborated by several observations. First, Satb1 was required for *de novo* activation of T_{reg}-SEs but not for the maintenance of established common-SEs. Second, the molecule could bind to closed chromatin at the DP stage, and the bound sites later became accessible and occupied by transcription factors in T_{reg} cells. Third, it was required for early stages of T_{reg} cell development but dispensable in differentiated T_{reg} cells. Given that Satb1 is highly expressed and bound to the T_{reg}-SEs from the DP stage[23,24], it is likely that Satb1 binding is a prerequisite for subsequent T_{reg}-SE activation upon appropriate signal transduction in developing thymic T_{reg} cells. In contrast, in differentiated T_{reg} cells, the repression of Satb1 appears to be necessary to prevent T_{reg} cells from acquiring helper T cell characteristics, presumably because Satb1 might cause unwanted chromatin reorganization when unduly expressed[37].

Our studies in T cell–specific Satb1-deficient mice revealed a correlation between impaired T_{reg}-SE activation and defective induction of T_{reg} signature genes, including *Foxp3*. Within the T_{reg}-SE at the *Foxp3* locus, Satb1 strongly bound to CNS0 before chromatin opening, and various transcription factors occupied this site along with Satb1-dependent enhancer activation. These properties of CNS0 suggest a role in initiating T_{reg}-SE activation to induce *Foxp3* expression. Indeed, deletion of this genomic region substantially impaired Foxp3 induction ((Y. Kitagawa, K.H., H. Watanabe, G. Kondoh and S.S., unpublished data). Other T_{reg} signature gene loci at which T_{reg}-SE activation and gene transcription were impaired by *Satb1* deletion included *Tnfrsf4*, which was shown to promote Foxp3 induction[38]. Although CD25 expression was similar between wild-type and Satb1-deficient tT_{reg} precursor cells, T_{reg}-SE activity and gene transcription at the *Il2ra* locus were substantially reduced by *Satb1* deletion, potentially destabilizing CD25 expression *in vivo* and interfering with tT_{reg} cell

differentiation, survival and proliferation[39]. These findings altogether suggest that Satb1-dependent T_{reg}-SE activation is required for priming tT_{reg} precursor cells to respond to cytokine and other signals and guiding relevant downstream transcription factors to the T_{reg} signature gene loci.

Satb1 deficiency in mature CD4SP thymocytes and T_{conv} cells derepressed *Foxp3* expression. Stage-specific *Satb1* deletion elicited T_{reg}-SE activation at the *Foxp3* locus, particularly around CNS0, before *Foxp3* de-repression. In addition, Satb1-deficient T_{conv} cells with derepressed *Foxp3* expression were converted more efficiently *in vivo* into stable pT_{reg} cells than were wild-type T_{conv} cells. Thus, despite the distinct functions of Satb1 in tT_{reg} and pT_{reg} cell differentiation, T_{reg}-SE activation is a common mechanism triggering Foxp3 expression. This finding can be exploited in a clinical setting to generate T_{reg} cells from T_{conv} cells via targeting Satb1.

Last, our findings indicate that defects in T_{reg}-SE formation could be a potential cause of autoimmune and other immunological diseases. *Satb1*$^{fl/fl}$*Cd4*-Cre^{+} mice developed multi-organ autoimmunity similar to that observed with neonatal tT_{reg} cell deficiencies induced by other means[27,40]. The reduction of disease severity by neonatal transfer of T_{reg} cells suggests that tT_{reg} cell deficiency and consequent reduction in total T_{reg} cell percentage in neonatal period was a major cause of the disease. Furthermore, the human *SATB1* locus contains single nucleotide polymorphisms (SNPs) associated with autoimmune diseases such as inflammatory bowel disease, psoriasis and multiple sclerosis[41] (GWAS Central, http://www.gwascentral.org, accessed 23 September 2015). Given that disease-associated SNPs are also enriched at cell type–specific SEs in various human cell types[14,16], these findings suggest that altered establishment of T_{reg}-SEs might contribute to genetic susceptibility to various immunological diseases via affecting T_{reg} cell differentiation.

In conclusion, the present study strongly suggests that Satb1-dependent establishment of T_{reg}-SEs controls the expression of T_{reg} cell signature molecules, including Foxp3, during tT_{reg} cell development. Impairment of this epigenetic event in developing T_{reg} cells is associated with autoimmunity similar to that induced by tT_{reg} cell depletion. Further study of how T_{reg}-SEs are primed and activated would aid understanding of the molecular basis of T_{reg} cell differentiation and of autoimmune and other immunological diseases.

ONLINE METHODS

Mice

Male, 4-week-old C57BL/6J mice (CLEA Japan) were used for preparing thymocyte subpopulations, and peripheral T_{conv} and T_{reg} cells for transcription factor chromatin immunoprecipitation sequencing (ChIP-seq). Male, 4-week-old *Foxp3-IRES-DTR/GFP* knock-in (*Foxp3*^{GFP}) mice (C57BL/6J), which express GFP under the endogenous *Foxp3* promoter without disrupting Foxp3 expression[42], were used to purify subpopulations of thymocytes and peripheral T cells for histone ChIP-seq, MBD-seq, ATAC-seq and RNA-seq. *Satb1* conditional knockout mice were prepared by crossing previously described *Satb1*$^{fl/fl}$ mice[26] with *Cd4*-Cre^{+} mice[43], *Foxp3*-Cre^{+} mice[44] or *Thpok*-Cre^{+} mice[32] (C57BL/6J). *Satb1*$^{fl/fl}$*Cd4*-Cre^{+} and *Satb1*$^{fl/fl}$*Thpok*-Cre^{+} mice were crossed with *Foxp3*^{GFP} mice to

isolate thymocyte or peripheral T cell subpopulations. For the Foxp3 induction assay using tT_{reg} precursor cells, *Satb1*$^{fl/fl}$*Cd4*-Cre^{+} mice were backcrossed to BALB/c background 10 times and further crossed with previously described *Foxp3*-eGFP fusion knock-in mice[45] to create a system where Foxp3 induction is perfectly mirrored by GFP expression. OT-II and RIP-OVA mice were previously described[46,47]. All mice used were maintained under specific pathogen-free conditions and all experiments were performed in accordance with guidelines for animal welfare set by Osaka University.

Cell preparation

For the preparation of double-positive (DP) thymocytes, CD4^{+}CD8^{+} cells were sorted from total thymocytes using FACSAria II (BD Biosciences). For sorting immature CD4 single-positive (imCD4SP; CD3ε^{+}CD4^{+}CD8^{-}CD24^{+}CD25^{-}GFP^{-}), tT_{reg} precursor (pre-tT_{reg}; CD3ε^{+}CD4^{+}CD8^{-}CD24^{+}CD25^{+}GITR^{+}GFP^{-}), thymic T_{reg} (thyT_{reg}; CD3ε^{+}CD4^{+}CD8^{-}CD25^{+}GFP^{+}) cells from the thymus of *Foxp3-DTR/GFP* knock-in mice, CD8^{-} thymocytes were first enriched by 'panning'—i.e., thymocytes stained with rat anti-CD8α antibody (BD Biosciences, clone 53-6.7) were incubated on a dish coated with goat anti-rat IgG antibody (MP Biomedicals). Nonadherent cells were stained with relevant antibodies and sorted by FACSAria II. Peripheral conventional T (T_{conv}; CD4^{+}CD25^{-}GFP^{-}) and T_{reg} (CD4^{+}CD25^{+}GFP^{+}) cells were sorted similarly, with prior removal of CD8^{+} and B220^{+} cells from lymphocytes and splenocytes. For the preparation of thymocyte subpopulations for Satb1 ChIP-seq, thymocytes were enriched and FACS-sorted from wild-type mice, and CD25^{-}CD4SP thymocytes and CD25^{+}CD4SP thymocytes (mixture of pre-tT_{reg} and thymic T_{reg} cells) were treated as immature CD4SP thymocytes and developing tT_{reg} cells, respectively. The following antibodies were used for FACS sorting: anti-CD4-APC (1:200, BD Biosciences), anti-CD8α-PerCP (1:200, BD Biosciences), anti-CD3ε-V500 (1:200, BD Biosciences), anti-CD24-BV421 (1:200, BioLegend), anti-CD25-PE (1:100, BD Biosciences) and anti-GITR-PE-Cy7 (1:200, BD Biosciences). Clone numbers were as follows: anti-CD4-APC (clone RM4-5), anti-CD8-PerCP (clone 53-6.7), anti-CD3e-V500 (clone 500A2), anti-CD24-BV421 (clone M1/69), anti-CD25-PE (clone PC61), anti-GITR-PE-Cy7 (clone DTA-1).

For the separation of peripheral T_{conv} and T_{reg} cells from pooled lymphocytes and splenocytes for transcription factor ChIP-seq, CD4^{+}CD25^{+} Regulatory T Cell Isolation Kit (Miltenyi Biotec) and CD4 (L3T4) Microbeads (Miltenyi Biotec) were used according to the manufacturer's instructions.

Activated T_{conv} and T_{reg} cells (Fig. 1h) were prepared by stimulating FACS-sorted T_{conv} and T_{reg} cells with Dynabeads Mouse T-Activator CD3/CD28 (Thermo Fisher) in RPMI 1640 supplemented with 10% FBS, penicillin–streptomycin, 2-mercaptoethanol and 30 or 100 U/ml IL-2, respectively, for 72 h.

ChIP-seq

For histone ChIP-seq and transcription factor ChIP-seq, 0.5–3 × 10^{5} and 2–10 × 10^{6} cells were used, respectively. Antibodies used were anti-H3K27ac (GeneTex, GEX60815), anti-H3K4me1 (ActiveMotif, 39297), anti-H3K27me3 (Millipore, 07-449), anti-H3K4me3

(Abcam, ab1012), anti-Satb1 (Abcam, ab70004), anti-Foxp3 (Abcam, 150743), anti-Runx1 (Abcam, ab23980), anti-CREB (Abcam, ab31387), anti-Ets1 (Santa Cruz, sc-350X), anti-Bcl11b (Bethyl Laboratories, A300-383A), anti-MED1 (Bethyl Laboratories, A300-793A), and anti-Smc1a (Bethyl Laboratories, A300-055A). Sorted cells were cross-linked in 1% (wt/vol) formaldehyde solution for 5 min (histone ChIP-seq) or 30 min (transcription factor ChIP-seq) and lysed. Cross-linked DNA was then fragmented by sonication using Digital Sonifier (Branson). The lysate was incubated overnight at 4 °C with 50–100 μl DynaBeads IgG magnetic beads (Thermo Fisher) that had been preincubated with 2.5–5 μg appropriate antibodies. Samples were washed, eluted, reverse cross-linked at 65 °C overnight, and purified using MinElute PCR Purification Kit (Qiagen). For transcription factor ChIP-seq, purified ChIP DNA was fragmented using Covaris Focused-ultrasonicator S220 (Covaris) before library preparation. Library was prepared using KAPA Library Preparation Kit Ion Torrent (KAPA Biosystems) according to the manufacturer's instructions and sequenced using Ion Proton (Thermo Fisher).

ChIP-seq reads were mapped to the mouse genome mm9 illumina iGenomes (http://support.illumina.com/sequencing/sequencing_software/igenome.html) using Bowtie2 (version 2.2.1). For visualization of ChIP peaks, MACS2.0 (version 10)[48] was used for peak calling, with input reads as control. ChIP-seq tracks were presented in GenomeJACK Browser (version 3.1, Mitsubishi Space Software). Owing to the variable signal-to-noise ratio among cell types (for example, tT_{reg} precursor cells are more apoptotic, and this tends to reduce signal-to-noise ratio), histone ChIP-seq peaks were normalized on the basis of the peak heights at the *Gapdh* locus when applicable, whereas other ChIP-seq peaks were normalized by total mapped read counts. For global analyses of histone ChIP-seq, raw tag counts were normalized using DESeq2 package (version 1.6.3) in R (version 3.1.2) (details are given below).

Identification of SEs and associated genes

H3K27ac ChIP-seq peaks were identified using FindPeaks in Homer package (version 4.7.2) with -region option, FDR set at 0.0001 and 40-fold enrichment over input. After removing peaks at promoter regions (within 2 kb of transcription start sites), H3K27ac peak density and clustering was assessed using ROSE[13,14]. Briefly, H3K27ac peaks within 12.5 kb of each other were stitched. Cumulative H3K27ac signal was determined for stitched enhancers and ranked by H3K27ac signal strength in ascending order. When stitched enhancer rank and H3K27ac signal strength were plotted in a lined scatter plot and both axes were scaled to 0 to 1, the point where the tangent of the curve = 1 was used to distinguish between SEs and TEs. Regions with enhancer rank higher and lower than this point were categorized as SEs and TEs, respectively. This process was carried out in duplicate, and regions intersecting in duplicates were defined as SEs for each cell type.

To identify SEs with statistically significant differences in H3K27ac intensity between T_{conv} and T_{reg} cells, we first normalized ChIP-seq tag counts in these enhancers as follows. On the basis of the assumption that the global H3K27ac signal is similar among cell types (as similarly assumed in quantitative ChIP-seq data analysis programs such as MAnorm)[49], mapped tags with MAPQ quality > 10 were counted for global H3K27ac peak regions and

normalized using DESeq2 package in R. Tag counts at combined stitched enhancers in the two cell types were normalized using the same normalization ratio as estimated by DESeq2 on the global peak regions. Using the resulting normalized tag counts, the data set was then analyzed for differential intensities of H3K27ac between the two populations, prepared in duplicate, using DESeq2. Differentially regulated SEs or TEs with FDR < 0.05 were defined as cell type–specific regions, and the rest were categorized as common regions. T_{reg}-SEs active in tT_{reg} precursor cells (Fig. 8a,b) were defined as those that showed a statistically significant increase in H3K27ac level in tT_{reg} precursor cells compared to DP thymocytes.

Enhancer-associated genes were defined as those located within 5 kb from both ends of the enhancer, on the basis of the calculation that median distance between genes in the mouse genome (mm9) is 13,726 bp and setting the limit at value smaller than half of median should theoretically determine which of the two neighboring genes an enhancer is assigned to. FPKM values <5 in all examined T cell populations (DP, imCD4SP, pre-tT_{reg}, $thyT_{reg}$, T_{reg} and T_{conv} cells) were filtered out, and this cutoff value was determined by distribution of FPKM values of global genes and the relative size of s.d. in duplicated samples.

Metagene representation

Similarly to the described method[14], average ChIP-seq density at merged SEs was presented by dividing SEs into 20 bins regardless of size, obtaining normalized tag counts for each bin and calculating the average for a group of SEs. Flanking 20-kb regions were also divided into 20 bins and average of normalized tag counts were calculated.

RNA-seq

For RNA-seq of DP, immature CD4SP, tT_{reg} precursor, thymic T_{reg}, T_{conv} and peripheral T_{reg} cells, 1×10^5 cells were sorted from *Foxp3*^{GFP} mice by FACSAria II and prepared for RNA-seq in duplicate. $CD4^+CD25^-$ cells from *Foxp3*^{GFP} and *Satb1*$^{fl/fl}$ *Thpok*-Cre^+ *Foxp3*^{GFP} mice were also sorted by FACSAria II, and 1×10^5 cells were used for RNA-seq. RNA was extracted using TRIzol Reagent (Thermo Fisher) and column purified using miRNeasy Micro Kit (Qiagen). RNA was subjected to library preparation with Ion Total RNA-Seq Kit v2 (Thermo Fisher) and sequenced by Ion Proton. Sequences were mapped to mm9 with TopHat2 (version 2.0.11). Normalized FPKM was generated with Cuffnorm (version 2.2.0) and differentially expressed genes (FDR < 0.05) were selected using Cuffdiff (version 2.2.0). T_{reg} up and down signature genes were defined as those that (i) are differentially expressed in peripheral T_{conv} and T_{reg} cells with FDR less than 0.05, (ii) have FPKM greater than 5 in either population, and (iii) have greater than threefold change in average FPKM of duplicates between T_{conv} and T_{reg} cells. For the selection of differentially expressed genes between tT_{reg} precursor and peripheral T_{reg} cells (Fig. 3a), FDR <0.05 was used. A list of genes associated with epigenetic modification was obtained from QuickGO GO:0006325 and GO:0040029.

For the comparison of T_{reg}-SE-associated gene expression (Supplementary Fig. 1g), RNA-seq data of various immune cell types were obtained from the NCBI database (GEO GSE60103)[50] and analyzed using the procedure described above.

RNA-seq of $CD24^+CD25^+GITR^+CD4SP$ thymocytes (developing T_{reg} cells, which include tT_{reg} precursor and immature thymic T_{reg} cells) and peripheral $CD4^+CD25^+GFP^+$ cells from *Satb1*$^{fl/+}$*Cd4*-Cre$^+$*Foxp3*^{GFP} and *Satb1*$^{fl/fl}$*Cd4*-Cre$^+$*Foxp3*^{GFP} mice was performed in duplicate with 10^3 cells. Cells were lysed in RLT buffer (Qiagen) and reverse transcribed using SMART-seq v4 Ultra Low Input RNA Kit for Sequencing (Clontech). cDNA was then fragmented by Covaris Focused-ultrasonicator S220, subjected to library preparation with KAPA Library Preparation Kit and sequenced by Ion Proton. Sequences were mapped to mm9 using Tophat2. Normalized FPKM was generated with Cuffnorm. For differential gene expression analyses, tag counts obtained by HT-seq (version 0.6.1) were analyzed using DESeq2 package in R (version 3.1.2).

Assay for transposase-accessible chromatin (ATAC)-seq

ATAC-seq was performed as described[51], with modifications to sequence using Ion Proton sequencing platform. Native chromatin transposed with sequencing adaptors using Nextera DNA Library Prep Kit (Illumina) was purified using a MinElute PCR Purification Kit (Qiagen). Purified DNA was amplified using NEBNext High-Fidelity PCR Master Mix (New England BioLabs) with the following primers: forward 5′-TCGTCGGCAGCGTCAGATGTG-3′ and reverse 5′-GTCTCGTGGGCTCGGAGATGT-3′. PCR fragments were size-selected (150–500 bp) with Agencourt AMPure XP (Beckman Coulter), sonicated by Covaris Focused-ultrasonicator S220, subjected to library preparation with KAPA Library Preparation Kit, and sequenced by Ion Proton. Sequence reads were mapped to mm9 using Bowtie2 after removal of PCR primer sequences by Cutadapt. ATAC-seq peaks were detected by MACS2.0 and visualized using GenomeJACK Browser, with peak height normalized at the *Gapdh* locus. Similarly to histone ChIP-seq, raw tag counts were normalized using DESeq2 package in R for global analyses.

Methyl-CpG binding domain protein (MBD)-seq

Genomic DNA, extracted from 10^6 FACS-sorted cells, was fragmented by Covaris focused-ultrasonicator S220, and fragments with methylated CpG were immunoprecipitated using MethylMiner Methylated DNA Enrichment Kit (Thermo Fisher). After purification with MinElute PCR Purification Kit, fragments were subjected to library preparation with KAPA Library Preparation Kit and sequenced by Ion Proton. Sequences were mapped to mm9, and peaks detected by MACS2.0 were visualized using GenomeJack Brower, with peak height normalized at the *Gapdh* locus. Global analyses were conducted based on normalized tag counts obtained using DESeq2 package in R. T_{reg}-specific DNA demethylated regions in Figure 1f were defined by comparing duplicated MBD-seq results in T_{conv} and T_{reg} cells using DiffBind package (version 1.12.3) in R. Regions with FDR < 0.005 and fold change > 3 were selected as differentially methylated regions.

Comparison between SEs and TEs

For the comparison of enhancer activity between T_{reg}-SEs and T_{reg}-TEs (Supplementary Fig. 2b), normalized tag counts at their constituents (unstitched H3K27ac peak regions) were used so that the sizes of included enhancer regions are normalized (median of T_{reg}-SE constituent size = 230 bp; median of T_{reg}-TE constituent size = 229 bp).

Detection of transcription factor-binding sites

Transcription factor ChIP-seq peaks were identified using FindPeaks, with their sizes fixed at 500 bp, minimum distance between peaks being 500 bp, and FDR set at 0.001. The overlap of SEs with ChIP-seq peaks or among transcription factor ChIP-seq peaks was defined by ≥ 1 bp overlap.

Categorization of Satb1-binding sites by the status of chromatin accessibility was based on the intersection between ATAC-seq peak sites (identified using FindPeaks, with -region option, minimum distance between peaks 100 bp, and FDR set at 0.00001) and Satb1-binding sites (Fig. 4b).

Binding of transcription factors at Satb1-binding sites was examined by calculating average tag counts per 10 million reads at ± 2 kb from the center of Satb1-binding sites, using annotatePeaks in Homer package (Fig. 4e).

Effects of *Satb1* deletion on T_{reg}-SE activation

H3K27ac ChIP-seq data of wild-type and ***Satb1***$^{fl/fl}$*Cd4*-Cre^{+} tT_{reg} precursor cells, prepared in duplicates, were analyzed for differential enhancer activity. Normalized tag counts at stitched enhancers, calculated following the procedure described above, were subjected to differential regulation test in DESeq2 package. Regions differentially regulated with FDR < 0.1 and fold change > 1.5 were defined as regions upregulated or downregulated by *Satb1* deletion.

Bidirectional enhancer RNA identification

Processed cap analysis gene expression (CAGE) data were obtained from FANTOM5 database (http://fantom.gsc.riken.jp/data/). Expression of bidirectional enhancer RNA was determined using the algorithm previously described[18], with tags mapped to exons and transcription start sites (TSS) excluded. Expression of bidirectional enhancer RNA was normalized by total read counts (Fig. 1c,e).

Microarray analysis

For analysis of gene expression in thymocyte fractions and other immune cells shown in Figure 3b, raw data from the NCBI database (GEO GSE15907) were analyzed[52].

Motif analysis

Satb1-binding sites (±100 bp) were subjected to known motif analysis, using findMotifsGenome in Homer package. Those with $P > 10^{-5}$ were considered as unreliable results (Supplementary Fig. 4b).

Flow cytometric analysis

Lymphocytes, splenocytes or thymocytes were subjected to Fc receptor blocking using purified anti-CD16/32 antibody (BioLegend), surface molecule staining with appropriate antibodies, and fixation and permeabilization using Foxp3/Transcription Factor Staining Buffer Set (Affymetrix eBioscience), followed by intracellular staining. Cytokine staining

was carried out after stimulation with 20 ng/ml phorbol myristate acetate (PMA), 709 ng/ml ionomycin and 0.67 μl/ml GolgiStop (BD Bioscience) for 4 h. Stained cells were analyzed using LSRFortessa (BD Bioscience). The following antibodies were used in addition to those mentioned above: anti-CD25-APC (1:100, eBioscience), anti-CD45.1-PE-Cy7 (1:200, BD Bioscience), anti-Foxp3-eFluor450 (1:100, eBioscience), anti-CTLA4-PE (1:100, BD Bioscience), anti-Helios-PE (1:100, BioLegend), anti-Nrp1-biotin (1:100, R&D Systems), and anti-IFN-γ-APC (1:200, Affymetrix eBioscience). Clone and catalog numbers were as follows: anti-CD25-APC (clone PC61.5) anti-CD45.1-PE-Cy7 (clone A20), anti-Foxp3-eFluor 450 (clone FJK-16s), anti-CTLA4-PE (clone UC10-4F10-11), anti-Helios-PE (clone 22F6), anti-Nrp1-biotin (catalog BAF566), anti-IFN-γ (clone XMG1.2). Dead cells were excluded from analyses by using Live/Dead Cell Viability Kit (Thermo Fisher).

Cell culture

The method for *in vitro* suppression assay (Supplementary Fig. 5a) was described[6]. Briefly, 5×10^4 peripheral T_{conv} cells, labeled with CellTrace Violet Proliferation Kit (Thermo Fisher) were incubated with 1 μg/ml anti-CD3ε antibody (BD Biosciences, 553057), 1×10^5 irradiated splenocytes and various ratios of $CD4^+CD25^+GFP^+$ T_{reg} cells from *Foxp3*^{GFP} or *Satb1*$^{fl/fl}$*Cd4*-Cre$^+$*Foxp3*^{GFP} mice in RPMI 1640 (Gibco) supplemented with 10% FBS, 0.05 mM 2-mercaptoethanol (Sigma-Aldrich), 100 U/ml penicillin and 100 μg/ml streptomycin (Gibco). Percentages of proliferated T_{conv} (responder) cells were analyzed using LSRFortessa after 4 d.

For the Foxp3 induction assay from tT_{reg} precursor cells, two protocols were used— one with IL-2 stimulation (Fig. 7c,d) and the other with IL-2 and TCR stimulation (Fig. 7e,f). For the former, similarly to the method described[8], $CD3\varepsilon^+CD24^+CD25^+GITR^+GFP^-CD4SP$ thymocytes from *Satb1*$^{fl/+}$*Cd4*-Cre$^+$*Foxp3*-eGFP and *Satb1*$^{fl/fl}$*Cd4*-Cre$^+$*Foxp3*-eGFP mice were incubated with 100 U/ml IL-2 for 24 h. For the latter, these cells were incubated with Dynabeads Mouse T-Activator CD3/CD28 (Thermo Fisher) in RPMI 1640 supplemented with 10% FBS, penicillin–streptomycin, 2-mercaptoethanol and 100 U/ml IL-2 for 5 d as described[9]. Percentages of $Foxp3^+$ cells were examined, and GFP^+ and GFP^- cells were sorted by FACSAria II for DNA demethylation assay.

The Foxp3 stability assay (Supplementary Figs. 5c and 7c) was performed by incubating target cells with Dynabeads Mouse T-Activator CD3/CD28 (Thermo Fisher) in RPMI 1640 supplemented with 10% FBS, penicillin–streptomycin and 2-mercaptoethanol, with or without 100 U/ml IL-2. Percentages of $Foxp3^+$ cells were analyzed after 6 d.

Immunoblotting

FACS-sorted cells were lysed and sonicated using Bioruptor UCD-200 (CosmoBio). Extracted protein was reduced, subjected to SDS-PAGE and transferred onto a PVDF membrane using iBlot2 (Thermo Fisher). Satb1 and GAPDH proteins were detected using anti-SATB1 antibody (BD Biosciences, 611182), HRP-conjugated anti-GAPDH antibody (Cell Signaling Technologies, 3683), HRP-conjugated anti-mouse IgG (GE Healthcare, NA931VS), ECL Prime Western Blotting Detection Reagent (GE Healthcare) and LAS-4000 mini (GE Healthcare).

ELISA

Serum samples from 16-week-old mice were collected by cardiac puncture and assessed for the level of serum immunoglobulin subtypes. Serum immunoglobulin was captured by anti-mouse Ig (Southern Biotech) and measured using HRP-conjugated anti-IgM, anti-IgG1, anti-IgG2c or anti-IgE (Southern Biotech) and TMB Substrate Reagent Set (BD Bioscience).

Generation of mixed bone marrow chimeric mice

T cell–depleted bone marrow cells from CD45.1$^+$ and CD45.2$^+$ *Satb1*$^{fl/fl}$*Cd4*-Cre$^+$ mice were mixed at a ratio of 2:1 (owing to the 'preferential' expansion of Satb1-deficient cells when mixed at 1:1 ratio) and injected intravenously in *Rag2*$^{-/-}$ mice, which had been irradiated at 3.5 Gy less than 24 h before transplantation.

Adoptive transfer of T_{reg} cells

FACS-sorted 1 × 10^6 peripheral CD4$^+$CD25$^+$ T_{reg} cells from 4- to 6-week-old wild-type mice (C57BL/6J) were adoptively transferred into 4-d-old *Satb1*$^{fl/fl}$*Cd4*-Cre$^+$ mice by intraperitoneal injection.

Histological analysis

Organs were harvested from 16-week-old mice and fixed in 10% formaldehyde for 1 week. They were embedded in paraffin, sectioned and stained with hematoxylin and eosin (H&E). Stained sections were subjected to scoring of disease severity, in a double-blinded manner, based on the following criteria.

Insulitis: 0, no insulitis; 1, peri-islet inflammation; 2, mild intra-islet insulitis; 3, severe intra-islet insulitis; 4, complete destruction of islets.

Oophoritis: 0, no oophoritis; 1, inflammatory cell infiltration; 2, tissue destruction with reduced oocytes; 3, tissue destruction with no oocytes or corpus luteum.

Sialdenitis: 0, no sialdenitis; 1, mild inflammation; 2, intermediate inflammation with up to 50% of area infiltrated; 3, severe inflammation with more than 50% of area infiltrated.

Gastritis: 0, no gastritis; 1, submucosal inflammation; 2, mild mucosal inflammation; 3, intermediate mucosal inflammation with destruction of gastric glands; 4, severe mucosal inflammation with loss of parietal cells.

Pneumonitis: 0, no pneumonitis; 1, mild inflammation; 2, intermediate inflammation; 3, severe inflammation and tissue destruction.

DNA methylation analysis by Sanger sequencing

Methods and primers for DNA methylation analysis for hypomethylated regions (Fig. 7e and Supplementary Figs. 5d and 6f) were described[6]. Briefly, genomic DNA extracted from 10^4–10^5 FACS-sorted cells was subjected to bisulfite treatment using MethylEasy Xceed (Human Genetic Signatures), followed by PCR amplification of target regions and subcloning into pTAC-1 plasmid in DynaExpress TA PCR Cloning Kit (BioDynamics Laboratory Inc). Amplicon sequence in plasmids were directly amplified from colonies using Illustra

TempliPhi Amplification Kit (GE Healthcare) and sequenced. 16 colonies per region were examined and average percentage of demethylated clones for each CpG residues in the amplicon sequence are shown in color code. Representative data of at least two independent experiments are shown.

DNA methylation analysis by deep sequencing

Genomic DNA was extracted from 1–5 × 10^5 FACS-sorted cells. Following bisulfite treatment with MethylEasy Xceed, *Foxp3* CNS2 region was amplified by PCR using KAPA HiFi HotStart Uracil$^+$ ReadyMix (KAPA Biosystems) and the following PCR primers: forward 5′-TTTTGGGTTTTTTTGGTATTTAAGA-3′ and reverse 5′-ACAAAT AATCTACCCCACAAATTTC-3′. PCR products were gel purified using MinElute Gel Extraction Kit (Qiagen). Approximately 500 ng purified amplicons was used for library construction with KAPA Library Preparation Kit according to the manufacturer's instructions (KAPA Biosystems) and sequenced using MiSeq (Illumina). To maximize the accuracy of sequencing, amplicons were mixed with random sequences so that the final amplicon percentage within a run was <5%. After quality trimming, sequence reads were mapped to mm9 using Bismark (version 0.13.1). Methylation status of 6 CpG residues contained in the amplicon sequence was visualized in color code using Methplot package (version 1.0) in R. Representative data of two independent experiments are shown (Fig. 5g and Supplementary Fig. 6h).

Colitis induction

CD4$^+$CD25$^-$CD45RB^{hi} T cells were FACS-sorted from CD45.1$^+$ wild-type or CD45.2$^+$ *Satb1*$^{fl/fl}$ *Thpok*-Cre$^+$ lymphocytes. 2.5 × 10^5 cells of each population were mixed and intravenously transferred into *Rag2*$^{-/-}$ mice. After 17 d, cells from mesenteric lymph nodes were isolated for FACS analysis, and CD45.1$^+$ or CD45.2$^+$ CD4$^+$ T cells were purified for DNA methylation analysis by amplicon sequencing.

Statistical analysis

Investigators estimated sample sizes on the basis of prior experience. Animals were selected randomly except for genotype and sex and were analyzed in a blinded manner. Experiments were independently replicated at least twice, and representative and/or summary data are shown. Flow cytometric analyses and DNA methylation analyses were independently repeated three or more times with three or more mice. All H3K27ac ChIP-seq and RNA-seq were prepared independently in two replicates, whereas other ChIP-seq experiments were performed once owing to the cost of sequencing. The number of experiments for representative images is stated in each figure legend. Variation in sample distribution was examined by Kolmogorov–Smirnov test. Statistical differences were determined by statistical tests stated in each Figure legend. $P < 0.05$ level of confidence was accepted for statistical significance.

Data availability

ChIP-seq, RNA-seq, MBD-seq and ATAC-seq data sets were deposited in DNA Data Bank of Japan under accession numbers DRA003955, DRA004738 and DRA005202.

Supplementary Material

Refer to Web version on PubMed Central for supplementary material.

Acknowledgments

We thank Y. Nakamura for DNA sequencing support and assistance with RNA-seq experiments, S. Kojo for providing technical advice regarding ChIP-seq experiments, and K. Chen for reading the manuscript. Bioinformatics analyses were conducted using the computer system at the Genome Information Research Center of the Research Institute for Microbial Diseases at Osaka University. This work was supported by Grants-in-Aid for Japanese Society for the Promotion of Science (JSPS) Fellows 261560 from the JSPS to Y.K. and Core Research for Evolutional Science and Technology from the Japan Science and Technology Agency to S.S. and JSPS Grants-in-Aid for Scientific Research B 15H04744 to N.O.

References

1. Sakaguchi S. Naturally arising $CD4^+$ regulatory T cells for immunologic self-tolerance and negative control of immune responses. Annu Rev Immunol. 2004; 22:531–562. [PubMed: 15032588]
2. Hori S, Nomura T, Sakaguchi S. Control of regulatory T cell development by the transcription factor Foxp3. Science. 2003; 299:1057–1061. [PubMed: 12522256]
3. Fontenot JD, Gavin MA, Rudensky AY. Foxp3 programs the development and function of $CD4^+CD25^+$ regulatory T cells. Nat Immunol. 2003; 4:330–336. [PubMed: 12612578]
4. Khattri R, Cox T, Yasayko SA, Ramsdell F. An essential role for Scurfin in $CD4^+CD25^+$ T regulatory cells. Nat Immunol. 2003; 4:337–342. [PubMed: 12612581]
5. Floess S, et al. Epigenetic control of the Foxp3 locus in regulatory T cells. PLoS Biol. 2007; 5:e38. [PubMed: 17298177]
6. Ohkura N, et al. T cell receptor stimulation-induced epigenetic changes and Foxp3 expression are independent and complementary events required for Treg cell development. Immunity. 2012; 37:785–799. [PubMed: 23123060]
7. Lee HM, Hsieh CS. Rare development of $Foxp3^+$ thymocytes in the $CD4^+CD8^+$ subset. J Immunol. 2009; 183:2261–2266. [PubMed: 19620303]
8. Lio CW, Hsieh CS. A two-step process for thymic regulatory T cell development. Immunity. 2008; 28:100–111. [PubMed: 18199417]
9. Toker A, et al. Active demethylation of the Foxp3 locus leads to the generation of stable regulatory T cells within the thymus. J Immunol. 2013; 190:3180–3188. [PubMed: 23420886]
10. Waddington, CH. The Strategy of the Genes: A Discussion of Some Aspects of Theoretical Biology. Allen and Unwin; 1957.
11. Davidson EH. Emerging properties of animal gene regulatory networks. Nature. 2010; 468:911–920. [PubMed: 21164479]
12. Arner E, et al. Transcribed enhancers lead waves of coordinated transcription in transitioning mammalian cells. Science. 2015; 347:1010–1014. [PubMed: 25678556]
13. Whyte WA, et al. Master transcription factors and mediator establish super-enhancers at key cell identity genes. Cell. 2013; 153:307–319. [PubMed: 23582322]
14. Hnisz D, et al. Super-enhancers in the control of cell identity and disease. Cell. 2013; 155:934–947. [PubMed: 24119843]
15. Adam RC, et al. Pioneer factors govern super-enhancer dynamics in stem cell plasticity and lineage choice. Nature. 2015; 521:366–370. [PubMed: 25799994]
16. Vahedi G, et al. Super-enhancers delineate disease-associated regulatory nodes in T cells. Nature. 2015; 520:558–562. [PubMed: 25686607]
17. Rada-Iglesias A, et al. A unique chromatin signature uncovers early developmental enhancers in humans. Nature. 2011; 470:279–283. [PubMed: 21160473]
18. Andersson R, et al. An atlas of active enhancers across human cell types and tissues. Nature. 2014; 507:455–461. [PubMed: 24670763]

19. Huehn J, Beyer M. Epigenetic and transcriptional control of Foxp3^{+} regulatory T cells. Semin Immunol. 2015; 27:10–18. [PubMed: 25801206]
20. Kagey MH, et al. Mediator and cohesin connect gene expression and chromatin architecture. Nature. 2010; 467:430–435. [PubMed: 20720539]
21. Magnani L, Eeckhoute J, Lupien M. Pioneer factors: directing transcriptional regulators within the chromatin environment. Trends Genet. 2011; 27:465–474. [PubMed: 21885149]
22. Zaret KS, Carroll JS. Pioneer transcription factors: establishing competence for gene expression. Genes Dev. 2011; 25:2227–2241. [PubMed: 22056668]
23. Yasui D, Miyano M, Cai S, Varga-Weisz P, Kohwi-Shigematsu T. SATB1 targets chromatin remodelling to regulate genes over long distances. Nature. 2002; 419:641–645. [PubMed: 12374985]
24. Cai S, Lee CC, Kohwi-Shigematsu T. SATB1 packages densely looped, transcriptionally active chromatin for coordinated expression of cytokine genes. Nat Genet. 2006; 38:1278–1288. [PubMed: 17057718]
25. Feng Y, et al. A mechanism for expansion of regulatory T-cell repertoire and its role in self-tolerance. Nature. 2015; 528:132–136. [PubMed: 26605529]
26. Hao B, et al. An anti-silencer- and SATB1-dependent chromatin hub regulates *Rag1* and *Rag2* gene expression during thymocyte development. J Exp Med. 2015; 212:809–824. [PubMed: 25847946]
27. Yang S, Fujikado N, Kolodin D, Benoist C, Mathis D. Immune tolerance. Regulatory T cells generated early in life play a distinct role in maintaining self-tolerance. Science. 2015; 348:589–594. [PubMed: 25791085]
28. Yadav M, et al. Neuropilin-1 distinguishes natural and inducible regulatory T cells among regulatory T cell subsets *in vivo*. J Exp Med. 2012; 209:1713–1722. [PubMed: 22966003]
29. Weiss JM, et al. Neuropilin 1 is expressed on thymus-derived natural regulatory T cells, but not mucosa-generated induced Foxp3^{+} T reg cells. J Exp Med. 2012; 209:1723–1742. [PubMed: 22966001]
30. Singh K, Hjort M, Thorvaldson L, Sandler S. Concomitant analysis of Helios and neuropilin-1 as a marker to detect thymic derived regulatory T cells in naïve mice. Sci Rep. 2015; 5:7767. [PubMed: 25586548]
31. Thiault N, et al. Peripheral regulatory T lymphocytes recirculating to the thymus suppress the development of their precursors. Nat Immunol. 2015; 16:628–634. [PubMed: 25939024]
32. Mucida D, et al. Transcriptional reprogramming of mature CD4^{+} helper T cells generates distinct MHC class II–restricted cytotoxic T lymphocytes. Nat Immunol. 2013; 14:281–289. [PubMed: 23334788]
33. Tai X, et al. Foxp3 transcription factor is proapoptotic and lethal to developing regulatory T cells unless counterbalanced by cytokine survival signals. Immunity. 2013; 38:1116–1128. [PubMed: 23746651]
34. Mousavi K, et al. eRNAs promote transcription by establishing chromatin accessibility at defined genomic loci. Mol Cell. 2013; 51:606–617. [PubMed: 23993744]
35. Gavin MA, et al. Foxp3-dependent programme of regulatory T-cell differentiation. Nature. 2007; 445:771–775. [PubMed: 17220874]
36. Morikawa H, et al. Differential roles of epigenetic changes and Foxp3 expression in regulatory T cell–specific transcriptional regulation. Proc Natl Acad Sci USA. 2014; 111:5289–5294. [PubMed: 24706905]
37. Beyer M, et al. Repression of the genome organizer SATB1 in regulatory T cells is required for suppressive function and inhibition of effector differentiation. Nat Immunol. 2011; 12:898–907. [PubMed: 21841785]
38. Mahmud SA, et al. Costimulation via the tumor-necrosis factor receptor superfamily couples TCR signal strength to the thymic differentiation of regulatory T cells. Nat Immunol. 2014; 15:473–481. [PubMed: 24633226]
39. Cheng G, Yu A, Dee MJ, Malek TR. IL-2R signaling is essential for functional maturation of regulatory T cells during thymic development. J Immunol. 2013; 190:1567–1575. [PubMed: 23315074]

40. Asano M, Toda M, Sakaguchi N, Sakaguchi S. Autoimmune disease as a consequence of developmental abnormality of a T cell subpopulation. J Exp Med. 1996; 184:387–396. [PubMed: 8760792]
41. Beecham AH, et al. Analysis of immune-related loci identifies 48 new susceptibility variants for multiple sclerosis. Nat Genet. 2013; 45:1353–1360. [PubMed: 24076602]
42. Kim JM, Rasmussen JP, Rudensky AY. Regulatory T cells prevent catastrophic autoimmunity throughout the lifespan of mice. Nat Immunol. 2007; 8:191–197. [PubMed: 17136045]
43. Lee PP, et al. A critical role for Dnmt1 and DNA methylation in T cell development, function, and survival. Immunity. 2001; 15:763–774. [PubMed: 11728338]
44. Wing K, et al. CTLA-4 control over Foxp3^{+} regulatory T cell function. Science. 2008; 322:271–275. [PubMed: 18845758]
45. Ito Y, et al. Detection of T cell responses to a ubiquitous cellular protein in autoimmune disease. Science. 2014; 346:363–368. [PubMed: 25324392]
46. Kurts C, et al. Constitutive class I-restricted exogenous presentation of self antigens in vivo. J Exp Med. 1996; 184:923–930. [PubMed: 9064352]
47. Barnden MJ, Allison J, Heath WR, Carbone FR. Defective TCR expression in transgenic mice constructed using cDNA-based α- and β-chain genes under the control of heterologous regulatory elements. Immunol Cell Biol. 1998; 76:34–40. [PubMed: 9553774]
48. Feng J, Liu T, Qin B, Zhang Y, Liu XS. Identifying ChIP-seq enrichment using MACS. Nat Protoc. 2012; 7:1728–1740. [PubMed: 22936215]
49. Shao Z, Zhang Y, Yuan GC, Orkin SH, Waxman DJ. MAnorm: a robust model for quantitative comparison of ChIP-Seq data sets. Genome Biol. 2012; 13:R16. [PubMed: 22424423]
50. Lara-Astiaso D, et al. Immunogenetics. Chromatin state dynamics during blood formation. Science. 2014; 345:943–949. [PubMed: 25103404]
51. Buenrostro JD, Giresi PG, Zaba LC, Chang HY, Greenleaf WJ. Transposition of native chromatin for fast and sensitive epigenomic profiling of open chromatin, DNA-binding proteins and nucleosome position. Nat Methods. 2013; 10:1213–1218. [PubMed: 24097267]
52. Mingueneau M, et al. The transcriptional landscape of αβ T cell differentiation. Nat Immunol. 2013; 14:619–632. [PubMed: 23644507]

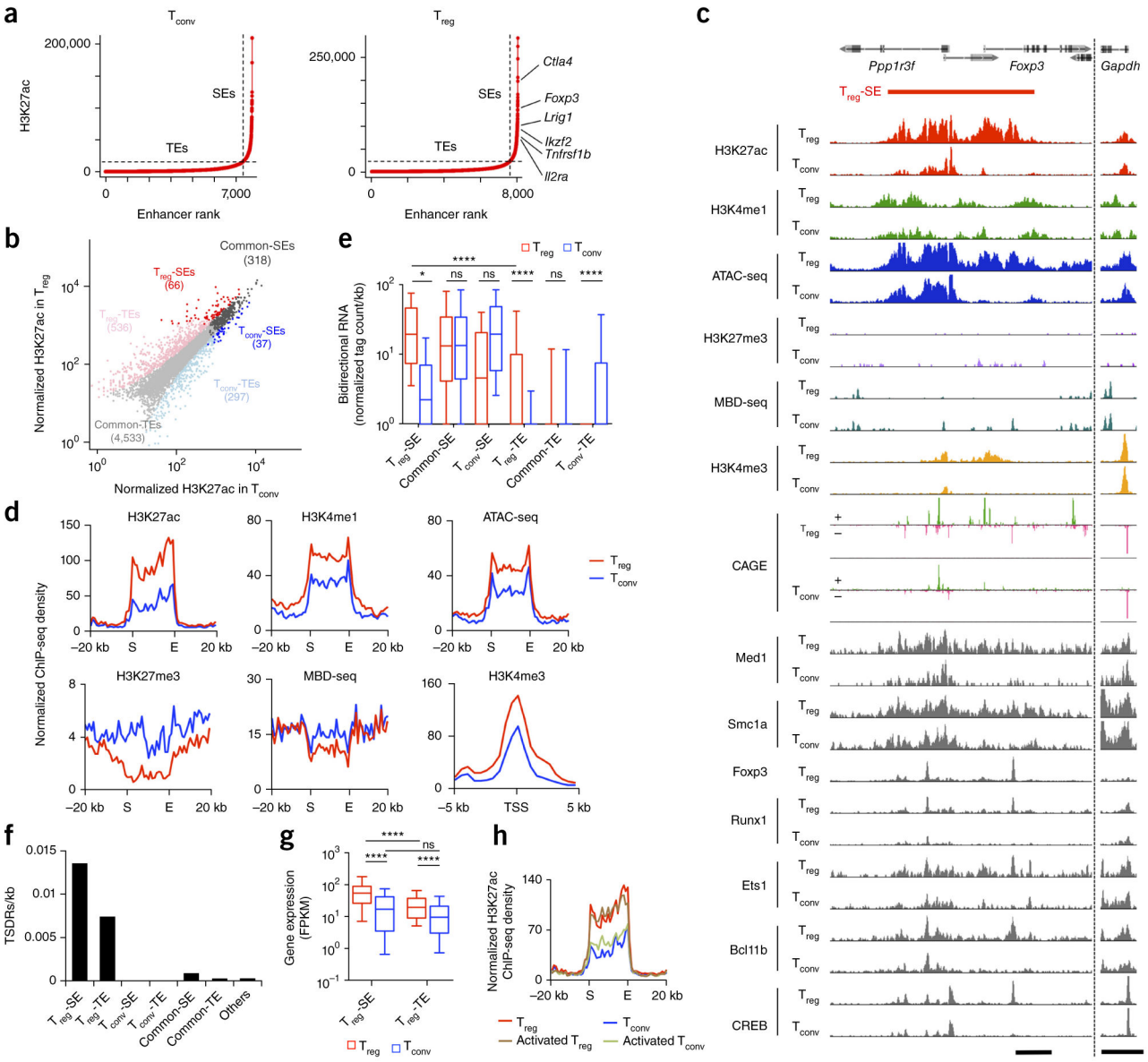

Figure 1.

Identification of T_{reg}-specific SEs. (**a**) Distribution of H3K27ac signals across the genome in peripheral T_{conv} and T_{reg} cells. Cumulative H3K27ac signals at stitched enhancers are plotted against enhancer rank. Dotted lines show the boundary between TEs and SEs. (**b**) Scatter plot showing normalized H3K27ac ChIP-seq tag counts at stitched enhancer regions in T_{conv} and T_{reg} cells. Numbers of regions in each category are shown in parentheses. (**c**) H3K27ac, H3K4me1, H3K27me3 and H3K4me3; ATAC-seq and MBD-seq signals; RNA transcription start sites assessed by cap analysis gene expression (CAGE) method; and binding of various transcription factors at the *Foxp3* T_{reg}-SE. Positive (+) and negative (−) strands are indicated for CAGE analysis. Peak heights are normalized at the *Gapdh* locus (right). Scale bars, 5 kb. (**d**) H3K27ac, H3K4me1 and H3K27me3; ATAC-seq; and MBD-seq signal at global T_{reg}-SE regions and H3K4me3 signal around transcription start sites

(TSS) of T_{reg}-SE-associated genes in T_{reg} and T_{conv} cells. Average normalized ChIP-seq density of 66 T_{reg}-SEs is plotted for merged T_{reg}-SE regions ± 20 kb or TSS ± 5 kb. Merged ends of T_{reg}-SEs are marked as S (start) and E (end). (**e**) Relative expression of bidirectional RNA produced from indicated regions in T_{reg} and T_{conv} cells. Box plots show median (center line), interquartile range (box) and tenth and ninetieth percentiles (whiskers). ns, $P > 0.05$; *$P \leq 0.05$; ****$P \leq 0.0001$ (Kruskal–Wallis test followed by Dunn's multiple comparisons test). (**f**) Frequency of T_{reg}-specific DNA hypomethylated regions (TSDRs). (**g**) Expression of genes associated with T_{reg}-SEs (61 genes) and T_{reg}-TEs (287 genes) in T_{conv} and T_{reg} cells. Average fragments per kilobase of transcript per million reads mapped (FPKM) of 2 independent RNA-seq experiments. Box plots show median (center line), interquartile range (box) and tenth and ninetieth percentiles (whiskers). ns, $P > 0.05$ and ****$P \leq 0.0001$ (Kruskal–Wallis test followed by Dunn's multiple comparisons test). (**h**) H3K27ac signals at merged T_{reg}-SE ± 20 kb (as in **d**) in T_{conv} and T_{reg} cells, before and after *in vitro* TCR stimulation with IL-2. Data are from 1 experiment (transcription factor ChIP-seq, ATAC-seq, H3K4me1 and H3K27me3 ChIP-seq), are representative of 2 independent experiments (H3K27ac ChIP-seq, H3K4me3 ChIP-seq and MBD-seq, **a**,**c**,**d**–**f**,**h**) or are the average of 2 independent experiments (RNA-seq, **b**,**g**).

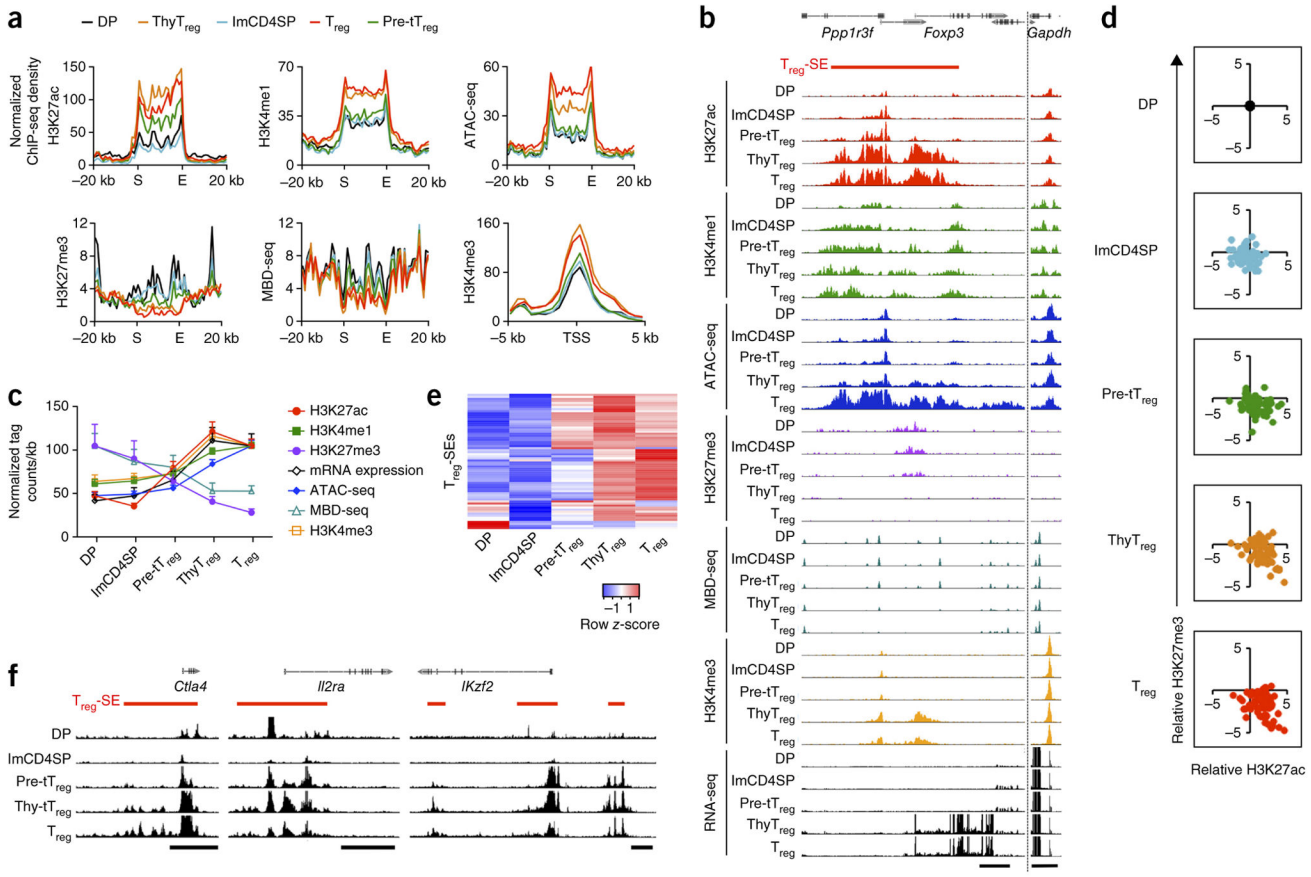

Figure 2.

Establishment of T_{reg}-specific SEs in developing T_{reg} cells. (**a**) H3K27ac, H3K4me1 and H3K27me3 and ATAC-seq and MBD-seq signals at global T_{reg}-SE regions and H3K4me3 signal around transcription start sites (TSS) of T_{reg}-SE-associated genes in DP thymocytes, immature CD4SP (imCD4SP) thymocytes and tT_{reg} precursor (pre-tT_{reg}), thymic T_{reg} ($thyT_{reg}$) and peripheral T_{reg} cells. Average normalized ChIP-seq density of 66 T_{reg}-SEs is plotted for merged T_{reg}-SE regions ± 20 kb or TSS ± 5 kb. Merged ends of T_{reg}-SEs are marked as S (start) and E (end). (**b**) Chromatin configuration changes of the T_{reg}-SE as in **a** and mRNA expression at the *Foxp3* locus during T_{reg} cell development. Peak heights are normalized at the *Gapdh* locus (right). Scale bars, 5 kb. (**c**) Changes in H3K27ac, H3K27me3, H3K4me1, ATAC-seq and MBD-seq signals at T_{reg}-SE regions, in H3K4me3 signal at TSS ± 5 kb of T_{reg}-SE-associated genes and in mRNA transcription of these genes during T_{reg} cell development. Mean normalized tag counts per kb ± s.e.m. of 66 T_{reg}-SE regions are plotted. (**d**) Scatter plots showing changes in H3K27ac (*x* axis) and H3K27me3 (*y* axis) signals at each T_{reg}-SE during T_{reg} cell development relative to those at the DP stage. Each dot indicates a T_{reg}-SE region. (**e**) Heat map of H3K27ac intensity of each T_{reg}-SE (rows) in indicated cell types (columns). Row *z*-score is shown in color gradient. (**f**) Changes in H3K27ac modifications in T_{reg}-SEs at T_{reg} signature gene loci during tT_{reg} cell development. Scale bars, 25 kb. Data are from 1 experiment (transcription factor ChIP-seq, ATAC-seq, H3K4me1 and H3K27me3 ChIP-seq), are representative of 2 independent

experiments (H3K27ac ChIP-seq, H3K4me3 ChIP-seq and MBD-seq), or are the average of 2 independent experiments (RNA-seq) (**a**–**f**).

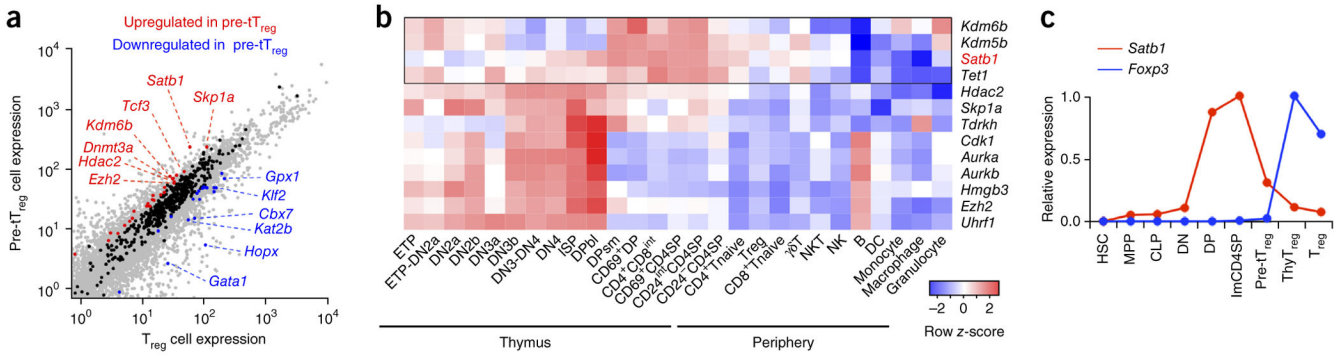

Figure 3.

Satb1 expression in T_{reg} precursor cells and binding to T_{reg}-SEs. (**a**) Differential expression of genes encoding epigenetic modifiers in tT_{reg} precursor (pre-tT_{reg}) and peripheral T_{reg} cells. Epigenetic modification–associated genes that are upregulated and downregulated in pre-tT_{reg} cells are highlighted in red and blue, respectively, and those that show similar expression are shown in black. (**b**) Relative expression of epigenetic modifiers upregulated in pre-tT_{reg} cells throughout thymocyte development and in various immune cells. Those with uniform gene expression patterns (variance < 0.5) were excluded, and row *z*-score is shown in heat map. (**c**) Relative mRNA expression of *Satb1* and *Foxp3* during T_{reg} cell development. ETP, early T cell lineage progenitor; ISP, immature SP; DPbl, DP blasts; DPsm, small DP; HSC, hematopoietic stem cell; MPP, multipotent progenitor; CLP, common lymphoid progenitor. Average normalized values from 2 independent RNA-seq experiments (**a**,**c**) and averages of 3 independent microarray experiments for each cell type (**b**) are shown.

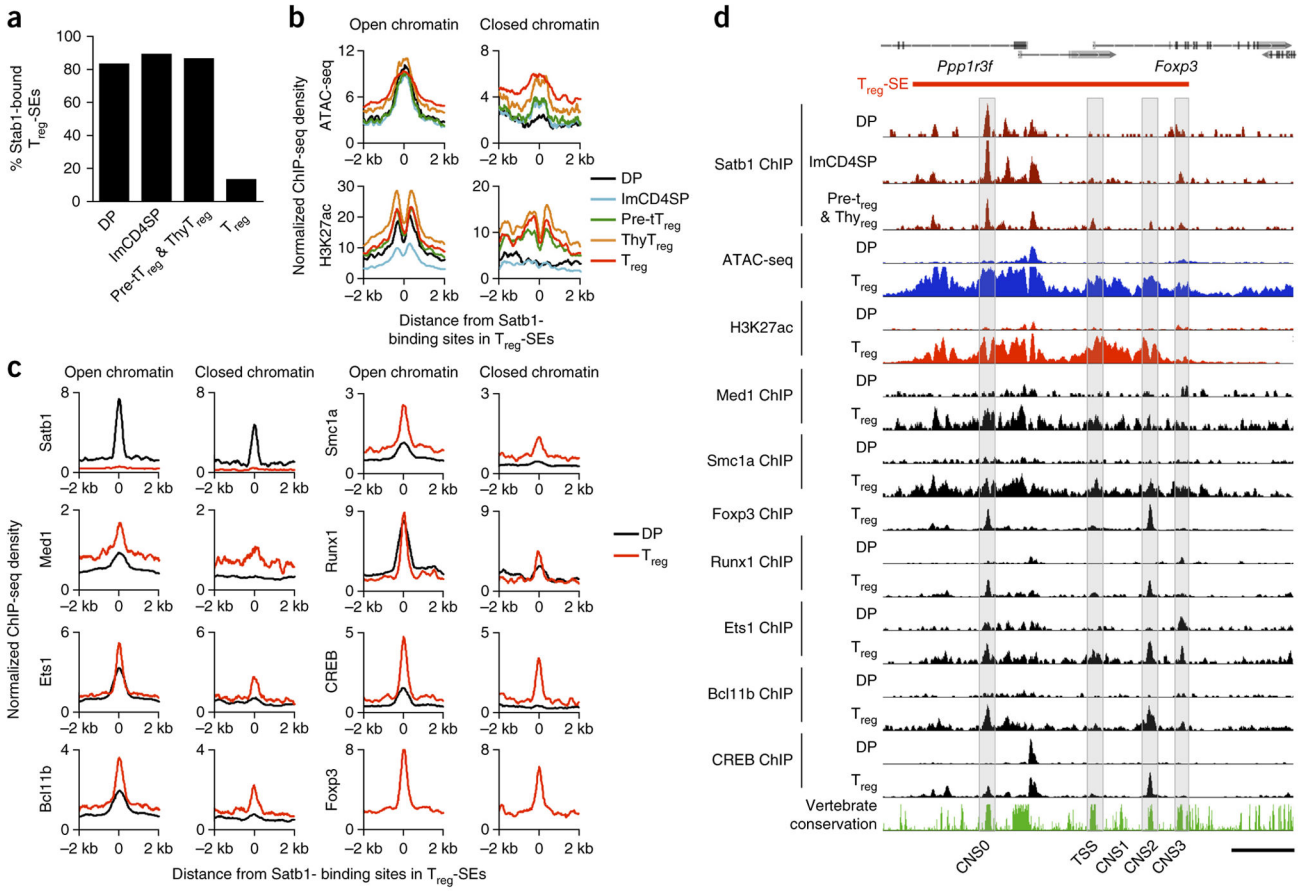

Figure 4.

Potential roles of Satb1 in activating T_{reg}-SEs. (**a**) Percentage of T_{reg}-SEs bound by Satb1 in DP, imCD4SP, a mixture of tT_{reg} precursor (pre-tT_{reg}) and thymic T_{reg} ($thyT_{reg}$) cells, and peripheral T_{reg} cells. (**b**) Chromatin accessibility and H3K27ac changes during T_{reg} cell development around sites where Satb1 bound at the DP stage in open or closed chromatin within T_{reg}-SEs. Average signal intensity of Satb1-binding sites (172 and 65 regions at open and closed chromatin, respectively) is shown for indicated cell types. (**c**) Density of indicated transcription factor binding in DP and peripheral T_{reg} cells around Satb1-binding sites at the DP stage in open or closed chromatin within T_{reg}-SEs. Normalized ChIP-seq signal density is plotted for Satb1-binding sites ± 2 kb. (**d**) Binding of Satb1 during tT_{reg} cell development and chromatin accessibility and transcription factor binding in DP and T_{reg} cells at the T_{reg}-SE of the *Foxp3* locus. Sequence conservation among vertebrates is also shown. The transcription start site (TSS) of the *Foxp3* gene and CNS are highlighted. Scale bar, 5 kb. Histone ChIP-seq data are representative of 2 independent experiments (**b**,**d**) and transcription factor ChIP-seq and ATAC-seq data are from 1 experiment (**a**–**d**).

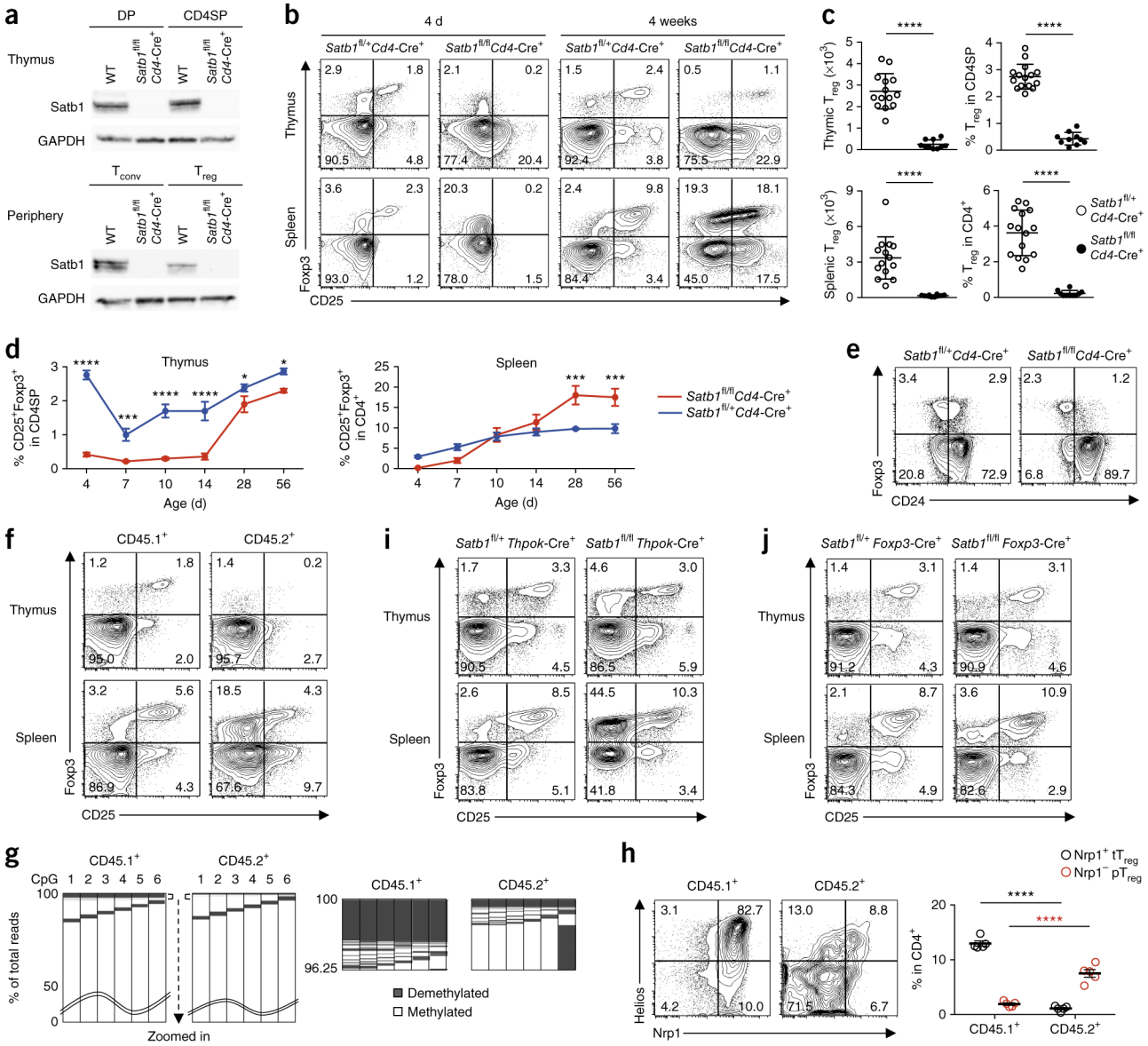

Figure 5.

Indispensable roles of Satb1 in tT_{reg} cell development. (**a**) Satb1 and GAPDH protein expression assessed by immunoblotting in DP thymocytes, CD4SP thymocytes and peripheral T_{conv} and T_{reg} cells from 4-week-old wild-type (WT) and *Satb1*$^{fl/fl}$*Cd4*-Cre^{+} mice. (**b**) Flow cytometry of CD4SP thymocytes and CD4^{+} splenocytes from 4-d-old and 4-week-old *Satb1*$^{fl/fl}$*Cd4*-Cre^{+} mice and littermate controls for identification of T_{reg} cells by the expression of Foxp3 and CD25. (**c**) Numbers and percentages of CD25^{+}Foxp3^{+} T_{reg} cells in the thymus and spleen of 4-d-old *Satb1*$^{fl/fl}$*Cd4*-Cre^{+} and littermate controls (mean ± s.e.m., n = 14, 10, 15 and 10). ****$P \leq 0.0001$ (two-tailed unpaired t-test). (**d**) Kinetics of T_{reg} cell accumulation in the thymus and spleen of *Satb1*$^{fl/fl}$*Cd4*-Cre^{+} mice and littermate controls. Percentage of CD25^{+}Foxp3^{+} T_{reg} cells among CD4SP thymocytes (left) and CD4^{+} splenocytes (right) are plotted (mean ± s.e.m., n = 6 per group). *$P \leq 0.05$; ***$P \leq 0.001$;

****$P \leq 0.0001$ (two-way ANOVA followed by Holm–Šídák multiple comparison test). (**e**) Flow cytometry of CD4SP thymocytes from 4-week-old *Satb1*$^{fl/fl}$*Cd4*-Cre^{+} mice and littermate controls for identification of CD24^{+}Foxp3^{+} immature T_{reg} cells. (**f**) Flow cytometry of CD45.1^{+} or CD45.2^{+} CD4SP thymocytes and CD4^{+} splenocytes from bone marrow chimeras generated with T cell–depleted bone marrow cells from WT (CD45.1^{+}) and *Satb1*$^{fl/fl}$*Cd4*-Cre^{+} (CD45.2^{+}) mice for identification of T_{reg} cells by Foxp3 and CD25 expression. (**g**) DNA methylation status of six CpG residues within *Foxp3* CNS2 in WT and Satb1-deficient CD4SP thymocytes from mixed bone marrow chimeras as in **f**, assessed by amplicon sequencing. CpGs are numbered 1–6 from the 5′ end (columns) and amplicons are ordered according to degree of demethylation (rows). Demethylated or methylated status is indicated by color code; waved lines (top) indicate the 0–50% of fully methylated amplicons omitted for presentation. The top 3.75% of total reads, when ordered from most to least demethylated clones, are magnified (bottom). (**h**) Flow cytometry of CD25^{+}Foxp3^{+} T_{reg} cells from bone marrow chimeras as in **f** for the expression of Nrp1 and Helios (top) and percentages of Nrp1^{+}CD25^{+}Foxp3^{+} tT_{reg} and Nrp1^{-}CD25^{+}Foxp3^{+} pT_{reg} cells among CD45.1^{+} and CD45.2^{+} CD4^{+} T cells (mean ± s.e.m., $n = 4$) (bottom). ****$P \leq 0.0001$ (two-way ANOVA followed by Holm–Šídák multiple comparison test). (**i**) Flow cytometry of CD4SP thymocytes and CD4^{+} splenocytes from 4-week-old *Satb1*$^{fl/+}$*Thpok*-Cre^{+} and *Satb1*$^{fl/fl}$*Thpok*-Cre^{+} mice for identification of T_{reg} cells by the expression of Foxp3 and CD25. (**j**) Flow cytometry of CD4SP thymocytes and CD4^{+} splenocytes from 4-week-old *Satb1*$^{fl/+}$*Foxp3*-Cre^{+} and *Satb1*$^{fl/fl}$*Foxp3*-Cre^{+} mice for identification of T_{reg} cells by the expression of Foxp3 and CD25. Data are representative or the summary of 3 independent experiments with 3 or more mice (**a**–**f**,**h**–**j**) or are representative of 2 independent experiments with 2 mice (**g**). Quadrant numbers indicate the percentages of gated cells (**b**,**e**,**f**,**h**–**j**).

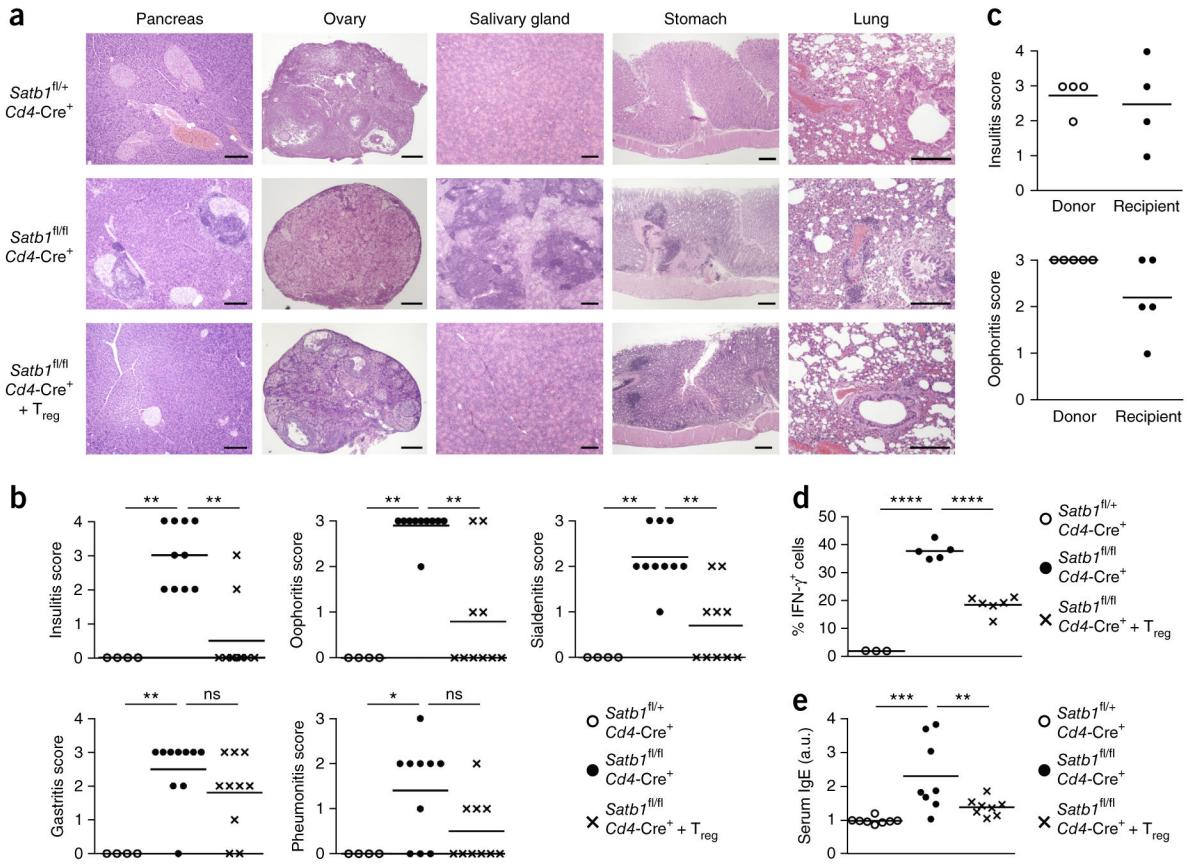

Figure 6.

Induction of autoimmunity by T cell–specific deletion of *Satb1*. (**a**) Hematoxylin and eosin staining of tissue sections from 16-week-old *Satb1*$^{fl/+}$*Cd4*-Cre^{+} mice ($n = 4$), *Satb1*$^{fl/fl}$*Cd4*-Cre^{+} mice ($n = 10$) and *Satb1*$^{fl/fl}$*Cd4*-Cre^{+} mice after 1×10^6 wild-type (WT) T_{reg} cell transfer on day 4 after birth ($n = 10$). Scale bars, 200 μm. (**b**) Severity of disease in mice shown in **a**. Horizontal lines indicate mean. ns, $P > 0.05$; $*P \leq 0.05$; $**P \leq 0.01$ (Kruskal–Wallis test followed by Dunn's multiple comparisons test). (**c**) Oophoritis and insulitis score of donor *Satb1*$^{fl/fl}$*Cd4*-Cre^{+} mice and *Rag2*$^{-/-}$ mice transferred with splenocytes from donor. Each recipient received cells from each donor. Horizontal lines indicate means. (**d**) Percentages of IFN-γ-producing cells among peripheral CD4^{+} non-T_{reg} cells in mice described in **a**. Horizontal lines indicate means ($n = 3$, 5 and 6 for *Satb1*$^{fl/+}$*Cd4*-Cre^{+}, *Satb1*$^{fl/fl}$*Cd4*-Cre^{+} and T_{reg}-transferred *Satb1*$^{fl/fl}$*Cd4*-Cre^{+} mice, respectively). $****P \leq 0.0001$ (ordinary one-way ANOVA, followed by Holm–Sidak multiple comparisons test). (**e**) Relative levels (arbitrary units (a.u.)) of serum IgE in mice shown in **a** ($n = 8$ per group). Horizontal lines indicate means. $**P \leq 0.01$ and $***P \leq 0.001$ (ordinary one-way ANOVA, followed by Holm–Šídák multiple comparisons test). Data are representative and summary of 4, 10 and 10 experiments for *Satb1*$^{fl/+}$*Cd4*-Cre^{+}, *Satb1*$^{fl/fl}$*Cd4*-Cre^{+} and *Satb1*$^{fl/fl}$*Cd4*-Cre^{+} with WT T_{reg} cell transfer independent experiments (**a**,**b**), summary of 4 or 5 independent experiments (**c**) or summary of 3 independent experiments (**d**,**e**).

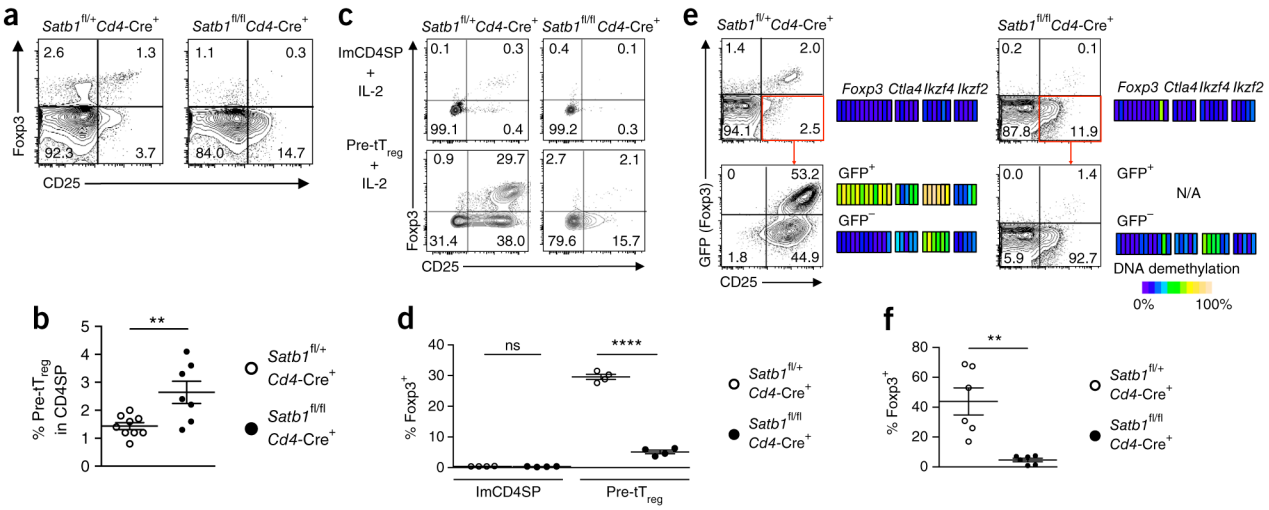

Figure 7.

Loss of T_{reg} differentiation potential in Satb1-deficient tTreg precursor cells. (**a**) Flow cytometry of CD24$^+$CD4SP thymocytes from 4-week-old *Satb1*$^{fl/fl}$*Cd4*-Cre$^+$ mice and littermate controls for identificationof tT_{reg} precursor (pre-tT_{reg}) cells by expression of CD25 and Foxp3. (**b**) Percentages of CD24$^+$CD25$^+$GITR$^+$Foxp3$^-$CD4SP tT_{reg} precursor cells in mice shown in **a** (mean ± s.e.m.; $n = 9$ and 7 *Satb1*$^{fl/+}$*Cd4*-Cre$^+$ and *Satb1*$^{fl/fl}$*Cd4*-Cre$^+$ mice, respectively). $^{**}P \leq 0.01$ (two-tailed unpaired *t*-test). (**c**,**d**) Flow cytometry of IL-2-stimulated immature CD4SP (imCD4SP) thymocytes and pre-tT_{reg} cells from *Satb1*$^{fl/+}$*Cd4*-Cre$^+$*Foxp3*^{GFP} or *Satb1*$^{fl/fl}$*Cd4*-Cre$^+$*Foxp3*^{GFP} mice for the expression of CD25 and Foxp3. Representative dot plots (**c**) and summary graph for the percentage of Foxp3$^+$ cells (**d**) are shown (mean ± s.e.m., $n = 4$). ns, $P > 0.05$; $^{****}P \leq 0.0001$ (ordinary one-way ANOVA, followed by Holm–Šídák multiple comparisons test). (**e**,**f**) Flow cytometry of IL-2- and TCR-stimulated pre-tT_{reg} cells from *Satb1*$^{fl/+}$*Cd4*-Cre$^+$*Foxp3*^{GFP} or *Satb1*$^{fl/fl}$*Cd4*-Cre$^+$*Foxp3*^{GFP} mice for the expression of CD25 and Foxp3. Representative dot plots (**e**) and summary graph (**f**) for the percentage of Foxp3$^+$ cells are shown (mean ± s.e.m., $n = 6$). Heat maps in **e** show DNA methylation status of T_{reg} signature genes in GFP$^+$ and GFP$^-$ cells before and after stimulation (N/A, data not available). Each block indicates an individual CpG in PCR-amplified regions. $^{**}P \leq 0.01$ (two-tailed unpaired *t*-test). Data are representative or summary of 3 (**a**,**b** and DNA methylation results in **e**), 2 (**c**,**d**) or 6 (**e**,**f**) independent experiments. Quadrant numbers indicate the percentages of gated cells (**a**,**c**,**e**).

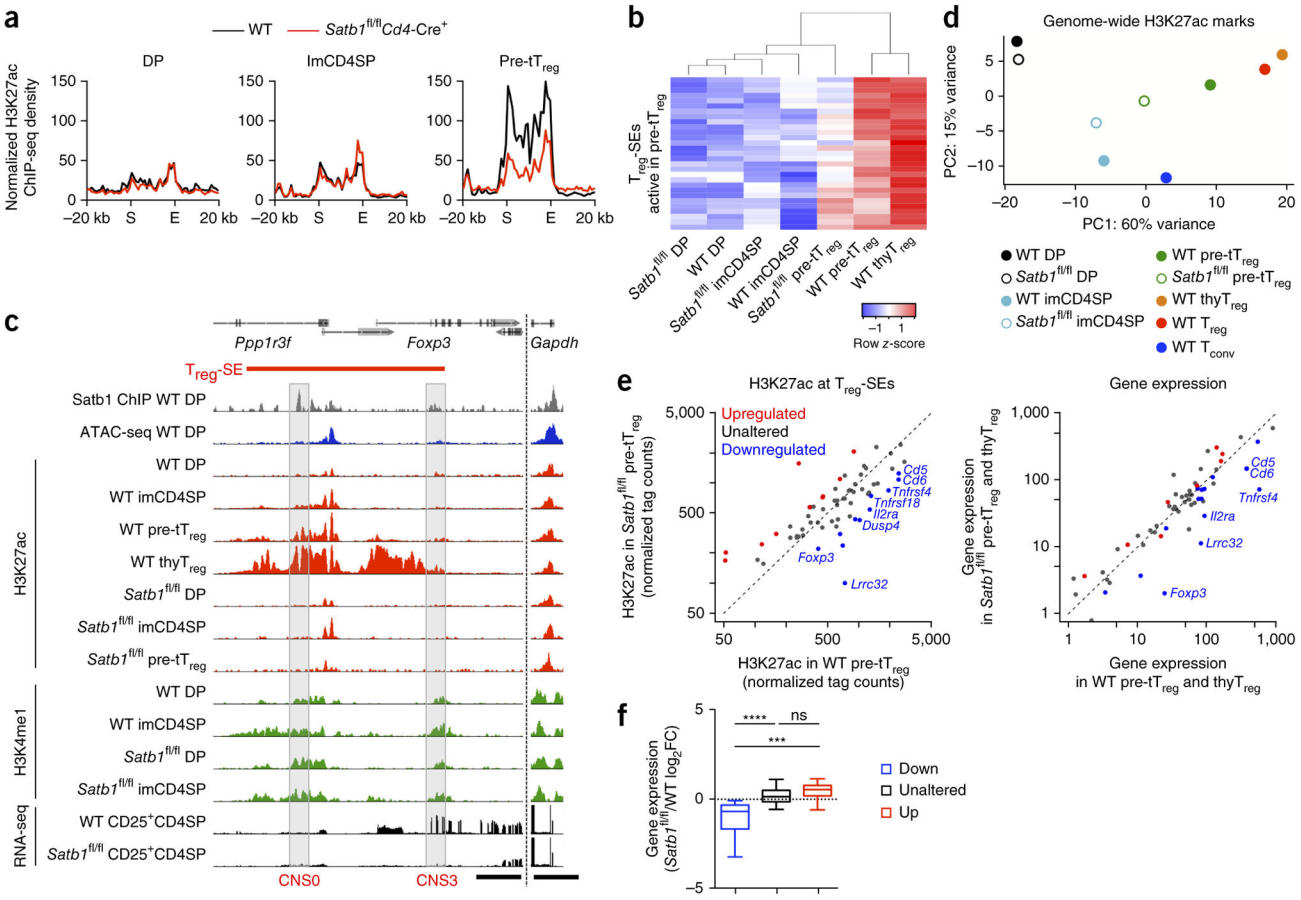

Figure 8.

Satb1-dependent T_{reg}-SE establishment and control of transcriptional changes in developing tT_{reg} cells. (**a**) H3K27ac signals of T_{reg}-SE regions in DP, immature CD4SP (imCD4SP) and tT_{reg} precursor (pre-tT_{reg}) cells from wild-type (WT) and *Satb1*$^{fl/fl}$*Cd4*-Cre^{+} mice. Average normalized ChIP-seq density of 29 T_{reg}-SE regions that are normally active in pre-tT_{reg} cells were calculated and plotted for merged T_{reg}-SE regions ± 20 kb. Merged ends of T_{reg}-SEs are marked as S (start) and E (end). (**b**) Heat map showing H3K27ac signal at each T_{reg}-SE (rows) in indicated cell types (columns), which are clustered by similarity. Row *z*-score is shown by color gradient. (**c**) H3K4me1 and H3K27ac modifications and mRNA transcription of the *Foxp3* locus in indicated cell types from WT and *Satb1*$^{fl/fl}$*Cd4*-Cre^{+} mice. Satb1-binding and chromatin accessibility in WT DP thymocytes are also shown. CNS0 and CNS3 regions are highlighted. Peak heights are normalized at the *Gapdh* locus. Scale bars, 5 kb. (**d**) Principal component analysis of global H3K27ac peaks in indicated cell populations. (**e**) Scatter plots showing changes in H3K27ac modifications of T_{reg}-SEs at the pre-tT_{reg} cell stage by Satb1 deficiency (left) and changes in T_{reg}-SE-associated gene expression in CD24^{+}CD25^{+}GITR^{+}CD4SP thymocytes (a mixture of pre-tT_{reg} and immature thymic T_{reg} ($thyT_{reg}$) cells) (right). T_{reg}-SEs are grouped according to the effects of Satb1 deficiency on their H3K27ac signal at the pre-tT_{reg} cell stage, and associated genes are highlighted in the gene expression plot. (**f**) Summary of effects of *Satb1* deletion on the expression of genes associated with T_{reg}-SEs whose H3K27ac signal is downregulated,

unaltered or upregulated by *Satb1* deletion as in **e** (15, 34 and 7 genes, respectively). Box plots show median (center line), interquartile range (box) and tenth and ninetieth percentiles (whiskers) of $\log_2$ fold-change between Satb1-deficient and WT mice. ns, $P > 0.05$; ***$P \leq 0.001$; ****$P \leq 0.0001$ (Kruskal–Wallis test, followed by Dunn's multiple comparisons test). H3K27ac ChIP-seq and RNA-seq data are representative of 2 independent experiments (**a**–**d**) or average of 2 independent experiments (**e**,**f**), and H3K4me1 ChIP-seq data are from 1 experiment (**c**).